

1 Isotopic constraints on heterogeneous sulfate production in Beijing haze

2 Pengzhen He¹, Becky Alexander², Lei Geng¹, Xiyuan Chi¹, Shidong Fan¹, Haicong Zhan¹, Hui Kang¹, Guangjie Zheng^{3†},
3 Yafang Cheng^{3,4}, Hang Su^{4,3}, Cheng Liu^{1,5,6}, Zhouqing Xie^{1,5,6*}

4 ¹Anhui Province Key Laboratory of Polar Environment and Global Change, School of Earth and Space Sciences, University
5 of Science and Technology of China, Hefei, Anhui 230026, China.

6 ²Department of Atmospheric Sciences, University of Washington, Seattle, WA 98195, USA.

7 ³Multiphase Chemistry Department, Max Planck Institute for Chemistry, Mainz 55128, Germany.

8 ⁴Jinan University, Institute for Environment and Climate Research, Guangzhou, Guangdong 511443, China.

9 ⁵Key Lab of Environmental Optics and Technology, Anhui Institute of Optics and Fine Mechanics, Chinese Academy of
10 Sciences, Hefei, Anhui 230031, China.

11 ⁶Center for Excellence in Urban Atmospheric Environment, Institute of Urban Environment, Chinese Academy of Sciences,
12 Xiamen, Fujian 361021, China.

13 *Corresponding to: Zhouqing Xie (zqxie@ustc.edu.cn)

14 †: Now at: Atmospheric Sciences Division, Brookhaven National Laboratory, Upton, NY 11973, USA.

15

16 **Abstract.** Discerning mechanisms of sulfate formation during fine-particle pollution (referred to as haze hereafter) in Beijing
17 is important for understanding the rapid evolution of haze and for developing cost-effective air pollution mitigation strategies.
18 Here we present observations of the oxygen-17 excess of PM_{2.5} sulfate ($\Delta^{17}\text{O}(\text{SO}_4^{2-})$) collected in Beijing haze from October
19 2014 to January 2015 to constrain possible sulfate formation pathways. Throughout the sampling campaign, the 12h-averaged
20 PM_{2.5} concentrations ranged from 16 to 323 $\mu\text{g m}^{-3}$ with a mean of $(141 \pm 88 (1\sigma)) \mu\text{g m}^{-3}$, with SO_4^{2-} representing 8–25 % of
21 PM_{2.5} mass. The observed $\Delta^{17}\text{O}(\text{SO}_4^{2-})$ varied from 0.1 ‰ to 1.6 ‰ with a mean of $(0.9 \pm 0.3) \text{‰}$. $\Delta^{17}\text{O}(\text{SO}_4^{2-})$ increased with
22 PM_{2.5} levels in October 2014 while the opposite trend was observed in November 2014 to January 2015. Our estimate
23 suggested that in-cloud reactions dominated sulfate production in polluted days (PD, $\text{PM}_{2.5} \geq 75 \mu\text{g m}^{-3}$) of Case II in October
24 2014 due to the relatively high cloud liquid water content, with a fractional contribution up to 68 %. During PD of Case I and
25 III–V, heterogeneous sulfate production (P_{het}) was estimated to contribute 41–54 % to total sulfate formation with a mean of
26 $(48 \pm 5) \%$. For the specific mechanisms of heterogeneous oxidation of SO_2 , chemical reaction kinetics calculations suggested
27 S(IV) (= $\text{SO}_2 \cdot \text{H}_2\text{O} + \text{HSO}_3^- + \text{SO}_3^{2-}$) oxidation by H_2O_2 in aerosol water accounted for 5–13 % of P_{het} . The relative importance
28 of heterogeneous sulfate production by other mechanisms was constrained by our observed $\Delta^{17}\text{O}(\text{SO}_4^{2-})$. Heterogeneous sulfate
29 production via S(IV) oxidation by O_3 was estimated to contribute 21–22 % of P_{het} on average. Heterogeneous sulfate
30 production pathways that result in zero- $\Delta^{17}\text{O}(\text{SO}_4^{2-})$, such as S(IV) oxidation by NO_2 in aerosol water and/or by O_2 via a radical

31 chain mechanism, contributed the remaining 66–73 % of P_{het} . The assumption about the thermodynamic state of aerosols
32 (stable or metastable) was found to significantly influence the calculated aerosol pH (7.6 ± 0.1 or 4.7 ± 1.1 , respectively), and
33 thus influence the relative importance of heterogeneous sulfate production via S(IV) oxidation by NO_2 and by O_2 . Our local
34 atmospheric conditions-based calculations suggest sulfate formation via NO_2 oxidation can be the dominant pathway in
35 aerosols at high pH-conditions calculated assuming stable state while S(IV) oxidation by O_2 can be the dominant pathway
36 providing that highly acidic aerosols ($\text{pH} \leq 3$) exist. Our local atmospheric conditions-based calculations illustrate the utility
37 of $\Delta^{17}\text{O}(\text{SO}_4^{2-})$ for quantifying sulfate formation pathways, but this estimate may be further improved with future regional
38 modelling work.

39 **1 Introduction**

40 Frequent occurrence of haze events in Beijing and throughout the North China Plain (NCP) during cold seasons is a health
41 threat for round 400 million people living there. High concentrations of $\text{PM}_{2.5}$ (particulate matter with an aerodynamic diameter
42 less than $2.5 \mu\text{m}$), of which the daily average can exceed $300 \mu\text{g m}^{-3}$ during severe haze (He et al., 2014; Jiang et al., 2015),
43 contribute to cardiovascular morbidity and mortality (Brook et al., 2010; Cheng et al., 2013). As one of the major components
44 of $\text{PM}_{2.5}$, sulfate is of particular concern due to its high concentrations in haze days (Zheng et al., 2015b; Zheng et al., 2015a)
45 and its key role in the climate system (Seinfeld and Pandis, 2006). Hourly sulfate concentrations can exceed $100 \mu\text{g m}^{-3}$ and
46 account for up to one quarter of $\text{PM}_{2.5}$ mass during severe haze (Zheng et al., 2015a). However, due to the generally low solar
47 radiation and cloud liquid water content during haze (Zheng et al., 2015a; Wang et al., 2014), conventional sulfate formation
48 via OH oxidation in the gas-phase and from aqueous-phase SO_2 (referred to as S(IV) = $\text{SO}_2 \cdot \text{H}_2\text{O} + \text{HSO}_3^- + \text{SO}_3^{2-}$) oxidation
49 by H_2O_2 (McArdle and Hoffmann, 1983), O_3 (Hoffmann and Calvert, 1985), and O_2 via a radical chain mechanism initiated
50 by transition metal ions (TMIs) in clouds (Ibusuki and Takeuchi, 1987; Alexander et al., 2009; Harris et al., 2013) cannot
51 explain the observed high sulfate concentrations (Zheng et al., 2015a). To explain the observed high sulfate concentrations
52 during haze in Beijing and NCP, recent studies have suggested that heterogeneous reactions on/in aerosols/aerosol water are
53 potentially important (He et al., 2014; Hung and Hoffmann, 2015; Cheng et al., 2016; Wang et al., 2016; Zheng et al., 2015a;
54 Zheng et al., 2015b; Wang et al., 2014). In particular, Zheng et al. (2015a) largely improved the underestimate of modelled
55 sulfate concentrations in 2013 Beijing haze by using a relative humidity-dependent uptake coefficient (γ) of SO_2 on aerosols,
56 without knowing the specific mechanisms of heterogeneous oxidation of SO_2 . Calculations by Guo et al. (2017) suggest
57 heterogeneous oxidation of SO_2 in Beijing maybe dominated by O_2 via a radical chain mechanism initiated by TMIs.
58 Laboratory work has suggested SO_2 oxidation by O_3 on mineral dust is a significant pathway for sulfate production (Li et al.,
59 2006), but its role in Beijing haze has not been determined. More recently, Hung and Hoffmann (2015) proposed that rapid
60 S(IV) oxidation by O_2 via a radical chain mechanism on acidic microdroplets ($\text{pH} \leq 3$) could be responsible for heterogeneous

61 sulfate production in Beijing haze, while Cheng et al. (2016) suggested that S(IV) oxidation by NO₂ (Lee and Schwartz, 1982;
62 Clifton et al., 1988) in aerosol water could be important due to the high relative humidity and NO₂ mole fraction during severe
63 haze in NCP. Due to the strong pH-dependence of SO₂ oxidation and the large variability of model calculated aerosol pH in
64 Beijing haze (Cheng et al., 2016; Wang et al., 2016; Liu et al., 2017), the relative importance of heterogeneous SO₂ oxidation
65 is difficult to constrain.

66 The oxygen-17 excess ($\Delta^{17}\text{O}$) of sulfate, defined as $\Delta^{17}\text{O} = \delta^{17}\text{O} - 0.52\delta^{18}\text{O}$, wherein $\delta = (R_{\text{sample}}/R_{\text{reference}} - 1)$ with R
67 representing the isotope ratios of ¹⁷O/¹⁶O or ¹⁸O/¹⁶O in the sample and the reference Vienna Standard Mean Ocean Water,
68 respectively (Matsuhisa et al., 1978), is a useful tool for estimating the relative importance of different sulfate formation
69 pathways because each oxidant transfers its $\Delta^{17}\text{O}$ signature to the product (Table 1) through SO₂ oxidation (Savarino et al.,
70 2000). SO₂ has $\Delta^{17}\text{O} = 0$ ‰ due to the rapid isotopic exchange with abundant vapour water whose $\Delta^{17}\text{O}$ is near 0 ‰ (Holt et
71 al., 1981). S(IV) oxidation by H₂O₂ and O₃ leads to $\Delta^{17}\text{O}(\text{SO}_4^{2-}) = 0.7$ ‰ and 6.5 ‰, respectively, on the basis of $\Delta^{17}\text{O}(\text{H}_2\text{O}_2)$
72 = 1.4 ‰ (Savarino and Thiemens, 1999) and assuming $\Delta^{17}\text{O}(\text{O}_3) = 26$ ‰ (Vicars and Savarino, 2014; Ishino et al., 2017).
73 Other sources of sulfate exhibit $\Delta^{17}\text{O}(\text{SO}_4^{2-})$ at or near 0 ‰. Specifically, sulfate directly emitted from natural and
74 anthropogenic sources or formed by OH and O₂ oxidation has $\Delta^{17}\text{O}(\text{SO}_4^{2-})$ values at or near 0 ‰ (Dubey et al., 1997; Luz and
75 Barkan, 2005; Lee et al., 2002; Bao et al., 2000). Sulfate produced by NO₂ oxidation is suggested to occur either via a radical
76 chain mechanism (Shen and Rochelle, 1998), via oxygen-atom transfer from OH⁻ (Clifton et al., 1988), or from O₂ based on
77 experimental results of He et al. (2014), resulting in $\Delta^{17}\text{O}(\text{SO}_4^{2-}) = 0$ ‰. Once formed, atmospheric sulfate does not undergo
78 further isotopic exchange, and $\Delta^{17}\text{O}(\text{SO}_4^{2-})$ will not be altered by mass-dependent processes such as deposition.

79 In this work, characteristics of PM_{2.5} $\Delta^{17}\text{O}(\text{SO}_4^{2-})$ during haze events from October 2014 to January 2015 in Beijing are
80 reported, contributions of O₃ and H₂O₂ oxidation in heterogeneous sulfate formation are quantified, and the roles of NO₂ and
81 O₂ oxidation are explored.

82 **2 Materials and Methods**

83 **2.1 Sampling and atmospheric observations**

84 A high volume air sampler (model TH-1000C II, Tianhong Instruments Co., Ltd, China) with quartz microfiber filter
85 (Whatman Inc., UK, pre-combusted at 450° C for 4 h) was used to collect PM_{2.5} samples at a flow rate of 1.05 m³ min⁻¹ from
86 October 2014 to January 2015. The collections lasted for 12 h (08:00–20:00 LT or 20:00–08:00 LT) for each sample. The
87 sample site is located on the rooftop of the First Teaching Building at the campus of University of the Chinese Academy of
88 Sciences (40.41° N, 116.68° E, around 20 m from the ground) in Beijing, around 60 km northeast of downtown. Hourly PM_{2.5}
89 concentration, SO₂, NO₂ and O₃ mole fractions were observed at Huairou station (40.33° N, 116.63° E) by Beijing Municipal
90 Environmental Monitoring Center, which is about 10 km from our aerosol sampling site. The mole fraction of atmospheric

91 H₂O₂ was not observed in our campaign, but long-term observations from March to November in Beijing shows a good
92 correlation between H₂O₂ mole fraction and air temperature (T in °C) according to $[\text{H}_2\text{O}_2]/(\text{nmol mol}^{-1}) = 0.1155e^{0.0846T/^\circ\text{C}}$. (Fu,
93 2014). In the present study, H₂O₂ mole fraction was estimated from our measured T with the above empirical equation. Our
94 calculated H₂O₂ mole fraction based on this formula in October and November 2014 is respectively (0.32 ± 0.08) nmol mol⁻¹
95 and (0.17 ± 0.04) nmol mol⁻¹, comparable to the observed values of (0.44 ± 0.18) nmol mol⁻¹ and (0.38 ± 0.11) nmol mol⁻¹,
96 respectively in October and November 2013 (Fu, 2014). Meteorological data including temperature, pressure and relative
97 humidity were recorded by an automatic weather station (model MetPak with integrated wind sonic, Gill Instruments Limited,
98 UK). Time reported in this paper is local time (LT = UTC + 8).

99 2.2 Measurements of ions and isotope ratios

100 The measurements of ions were conducted in Anhui Province Key Laboratory of Polar Environment and Global Change
101 in the University of Science and Technology of China. A detailed description of the method for chemical analysis of NH₄⁺,
102 K⁺, Ca²⁺, Na⁺, Mg²⁺, SO₄²⁻, NO₃⁻ and Cl⁻ can be found in the literature (Ye et al., 2015). Briefly, ions were extracted from a
103 part (2 cm × 2 cm) of each filter with 20 ml of Millipore water (≥ 18 M Ω) by sonication for 80 min in an ice water bath.
104 Insoluble substances in the extract were filtered with 0.45 μm filters before analysis. The pH of filtrates was measured by an
105 ion activity meter (model PXS-215, Shanghai INESA Scientific Instrument Co., Ltd., China). And the ion concentrations were
106 analysed using Dionex ICS-2100 ion chromatograph system (Thermo Fisher Scientific Inc., USA). Typical analytical precision
107 by our instrument is better than 10 % RSD (relative standard deviation) for all ions (Chen et al., 2016). The preparation and
108 measurements of $\Delta^{17}\text{O}(\text{SO}_4^{2-})$ were conducted in Isolab (<https://isolab.ess.washington.edu/isolab/>) at the University of
109 Washington, USA. A detailed description of the method can be found in the literature (Savarino et al., 2001; Geng et al., 2013;
110 Chen et al., 2016; Alexander et al., 2012). Briefly, PM_{2.5} sample filters were dissolved in Millipore water (≥ 18 M Ω) and the
111 insoluble substances were filtered. Pre-packed ion capture cartridges (Alltech Maxi-Clean IC-RP SPE) were used for the first
112 step of removal of organics. Cations in the samples were replaced with sodium using a cation exchange resin and 30 % H₂O₂
113 solution was added as the second step of removal of organics. Excess H₂O₂ was removed via evaporation and SO₄²⁻ was
114 separated from other anions (e.g., NO₃⁻) by ion chromatography. After ion separation, SO₄²⁻ was converted to Ag₂SO₄, dried,
115 and then pyrolyzed at 1000° C in an elemental analyzer to form Ag(s), SO₂(g), and O₂(g). The produced gases were carried by
116 He gas to pass through a liquid nitrogen trap to remove SO₂, and then a GC to further purify the O₂ gas which was finally
117 induced to a mass spectrometer (Thermo Scientific MAT 253). Masses of 32, 33 and 34 of O₂ were measured to determine
118 $\delta^{17}\text{O}$ and $\delta^{18}\text{O}$ and then $\Delta^{17}\text{O}$ was calculated. The typical amount of O₂ for each run is 0.4–0.8 μmol . The precision of $\Delta^{17}\text{O}$
119 measurements in our method is ± 0.3 % based on replicate analysis of standards, which is consistent with previous studies
120 (Alexander et al., 2005; Sofen et al., 2014; Chen et al., 2016). To quantify the uncertainty in each sample, 30 samples were
121 measured in triplicate, 2 samples in quadruplicate, and 2 samples in duplicate depending on the limitation of sample size. In

122 total, 10 filters sampled in non-polluted days (NPD, $PM_{2.5} < 75 \mu\text{g m}^{-3}$) and 24 filters sampled in polluted days (PD, $PM_{2.5} \geq$
 123 $75 \mu\text{g m}^{-3}$) were analysed.

124 2.3 Estimate of the overall rate of heterogeneous sulfate production

125 Heterogeneous sulfate production (P_{het}) is commonly parameterized in models according to Eq. (1) (Jacob, 2000; Zheng
 126 et al., 2015a):

$$127 P_{\text{het}} = \frac{3600 \text{ s h}^{-1} \times 96 \text{ g mol}^{-1} \times p}{RT} \left(\frac{R_p}{D_g} + \frac{4}{v\gamma} \right)^{-1} S_p [\text{SO}_2(\text{g})] \quad (1)$$

128 where P_{het} is in unit of $\mu\text{g m}^{-3} \text{ h}^{-1}$, 3600 s h^{-1} is a time conversion factor, 96 g mol^{-1} is the molar mass of SO_4^{2-} , p is atmospheric
 129 pressure in kPa, R is the gas constant ($8.31 \text{ Pa m}^3 \text{ mol}^{-1} \text{ K}^{-1}$), and T is temperature in K. R_p is the radius of aerosol particles
 130 (m), D_g is the gas-phase molecular diffusion coefficient of SO_2 ($\text{m}^2 \text{ s}^{-1}$), v is the mean molecular speed of SO_2 (g) (m s^{-1}), γ is
 131 the uptake coefficient of SO_2 on aerosols with the unit of 1, $[\text{SO}_2(\text{g})]$ is the gas-phase mole fraction of SO_2 (nmol mol^{-1}) and
 132 S_p is the aerosol surface area per unit volume of air ($\text{m}^2 \text{ m}^{-3}$). The typical tropospheric value of D_g and v is $2 \times 10^{-5} \text{ m}^2 \text{ s}^{-1}$ and
 133 300 m s^{-1} , respectively (Jacob, 2000). Observations of $PM_{2.5}$ mass concentrations ($c(\text{PM}_{2.5})$, $\mu\text{g m}^{-3}$) and $PM_{2.5}$ mean radius
 134 (m) during Beijing haze roughly follows an empirical formula: $R_p/m = (0.254c(\text{PM}_{2.5})/(\mu\text{g m}^{-3}) + 10.259) \times 10^{-9}$ (Guo et al.,
 135 2014). By using the volume and surface area formulas of a sphere and the mean density of particles $\rho = 1.5 \times 10^6 \text{ g m}^{-3}$ (Guo et
 136 al., 2014), S_p can be estimated from Eq. (2). A relative humidity-dependent γ ($= (2-5) \times 10^{-5}$, Eq. (3)) derived from Zheng et al.
 137 (2015a) during 2013 Beijing haze was used. This range of γ is also consistent with the estimated values of γ from (1.6 ± 0.7)
 138 $\times 10^{-5}$ to $(4.5 \pm 1.1) \times 10^{-5}$ by Wang et al. (2016).

$$139 S_p = \frac{c(\text{PM}_{2.5}) \times 10^{-6} \text{ g } \mu\text{g}^{-1}}{4/3 \times \pi R_p^3 \times \rho} \times 4\pi R_p^2 \quad (2)$$

$$140 \gamma = \begin{cases} 2 \times 10^{-5}, \Psi \leq 50 \% \\ 2 \times 10^{-5} + \frac{5 \times 10^{-5} - 2 \times 10^{-5}}{100\% - 50\%} \times (\Psi - 50\%), 50 \% \leq \Psi \leq 100 \% \end{cases} \quad (3)$$

141 where Ψ refers to relative humidity with the unit of %.

142 2.4 Estimate of primary sulfate

143 The primary sulfate, which is directly emitted into air, includes the sea salt source, terrigenous source and anthropogenic
 144 source (Li et al., 2013; Faloon, 2009). The concentration of sea salt sulfate was calculated by using the observed
 145 concentrations of Na^+ and the mass ratio of $c(\text{SO}_4^{2-})/c(\text{Na}^+) = 0.252$ in seawater (Calhoun et al., 1991). The terrigenous sulfate
 146 was estimated using the observed concentrations of Ca^{2+} and the mass ratio of $c(\text{SO}_4^{2-})/c(\text{Ca}^{2+}) = 0.18$ in soil (Legrand et al.,
 147 1997), where $c(\text{Ca}^{2+})/c(\text{Na}^+) = 0.038$ in seawater was used to calculate the fraction of observed Ca^{2+} from soil (Legrand and
 148 Mayewski, 1997). The anthropogenic primary sulfate is estimated as 3 % of anthropogenic SO_2 emissions in models (Faloon,
 149 2009; Alexander et al., 2009). Supposing all the observed mole fraction of SO_2 and precursors of secondary sulfate are

150 anthropogenic, we have $c(\text{ap})/96 = 0.03(c(\text{SO}_2)/64 + c(\text{sas})/96)$, where $c(\text{sas}) = c(\text{tos}) - c(\text{ss}) - c(\text{ts}) - c(\text{ap})$ and $c(\text{ap})$, $c(\text{sas})$, $c(\text{tos})$,
 151 $c(\text{ss})$ and $c(\text{ts})$ is the mass concentrations of anthropogenic primary sulfate (ap), secondary sulfate (sas), total sulfate (tos), sea
 152 salt sulfate (ss) and terrigenous sulfate (ts). The estimated concentration of total primary sulfate (p-SO_4^{2-}) is the sum of primary
 153 sulfate from all these sources.

154 2.5 Estimate of sulfate production rate from OH oxidation in the gas-phase

155 The sulfate production rate from OH oxidation in the gas-phase ($P_{\text{SO}_2+\text{OH}}$) can be expressed as:

$$156 P_{\text{SO}_2+\text{OH}} = \frac{3600 \text{ s h}^{-1} \times 96 \text{ g mol}^{-1} \times p \times R_{\text{SO}_2+\text{OH}}}{RT} \quad (4)$$

157 where $P_{\text{SO}_2+\text{OH}}$ is in unit of $\mu\text{g m}^{-3} \text{ h}^{-1}$, 3600 s h^{-1} , 96 g mol^{-1} , p , R and T is the same as Eq. (1). $R_{\text{SO}_2+\text{OH}}$ is the chemical reaction
 158 rate ($\text{nmol mol}^{-1} \text{ s}^{-1}$), calculated as shown in Table S1 and S2.

159 2.6 Estimate of in-cloud sulfate production rate

160 The main in-cloud sulfate formation pathways considered here include S(IV) oxidation by H_2O_2 , O_3 , NO_2 (Wang et al.,
 161 2016) and O_2 via a radical chain mechanism initiated by TMIs (Alexander et al., 2009). Their chemical reaction rate
 162 expressions ($R_{\text{S(IV)+oxi}}$) and rate constants (k) are summarized in Table S3. The rate of in-cloud sulfate production by a certain
 163 oxidant ($P_{\text{cloud, S(IV)+oxi}}$) can be expressed as (Seinfeld and Pandis, 2006):

$$164 P_{\text{cloud, S(IV)+oxi}} = 3600 \text{ s h}^{-1} \times 96 \text{ g mol}^{-1} \times R_{\text{S(IV)+oxi}} \times \frac{L_c}{\rho_w} \quad (5)$$

165 where $P_{\text{cloud, S(IV)+oxi}}$ is in unit of $\mu\text{g m}^{-3} \text{ h}^{-1}$, 3600 s h^{-1} and 96 g mol^{-1} is the same as Eq. (1), and $R_{\text{S(IV)+oxi}}$ is in unit of M s^{-1} .
 166 Cloud liquid water content (L_c , in unit of mg m^{-3}) was derived from a global reanalysis, GEOS-FP
 167 (<https://gmao.gsfc.nasa.gov/products/>). ρ_w is the density of water (1 kg L^{-1}). By summing in-cloud S(IV) oxidation by H_2O_2 ,
 168 O_3 , NO_2 and O_2 initiated by TMIs up, we can get the total rate of in-cloud sulfate production (P_{cloud}).

169 2.7 Isotopic constraints on sulfate formation pathways

170 Since S(IV) oxidation by O_3 and H_2O_2 are the sole sources of non-zero $\Delta^{17}\text{O}(\text{SO}_4^{2-})$ (Table 1) (Savarino et al., 2000), the
 171 relative importance of different sulfate formation pathways can be calculated as follows (Alexander et al., 2012):

$$172 \Delta^{17}\text{O}_{\text{obs}} = (6.5\% \times f_{\text{S(IV)+O}_3}) + (0.7\% \times f_{\text{S(IV)+H}_2\text{O}_2}) + (0 \times f_{\text{zero-}\Delta^{17}\text{O}}) \quad (6)$$

173 where $f_{\text{S(IV)+O}_3}$ and $f_{\text{S(IV)+H}_2\text{O}_2}$ are fractional contributions of S(IV) oxidation by O_3 and H_2O_2 to the observed sulfate, respectively,
 174 and $f_{\text{zero-}\Delta^{17}\text{O}}$ represents fractional contribution of sulfate with zero- $\Delta^{17}\text{O}$ processes such as primary sulfate, secondary sulfate
 175 formed via OH oxidation, NO_2 oxidation, and O_2 oxidation. By using Eq. (6) and the definition $f_{\text{S(IV)+O}_3} + f_{\text{S(IV)+H}_2\text{O}_2} + f_{\text{zero-}\Delta^{17}\text{O}}$
 176 $= 1$, we have $f_{\text{S(IV)+O}_3} = (\Delta^{17}\text{O}_{\text{obs}} - 0.7\% \times f_{\text{S(IV)+H}_2\text{O}_2}) / 6.5\%$ and $f_{\text{zero-}\Delta^{17}\text{O}} = (6.5\% - \Delta^{17}\text{O}_{\text{obs}} - 5.8\% \times f_{\text{S(IV)+H}_2\text{O}_2}) / 6.5\%$. Since $f_{\text{S(IV)+O}_3}$,
 177 $f_{\text{S(IV)+H}_2\text{O}_2}$, and $f_{\text{zero-}\Delta^{17}\text{O}}$ should be in the range of 0 to 1 at the same time, $f_{\text{S(IV)+H}_2\text{O}_2}$ is further limited to meet $f_{\text{S(IV)+H}_2\text{O}_2} <$

178 $\min\{\Delta^{17}\text{O}_{\text{obs}}/0.7\text{‰}, (6.5\text{‰}-\Delta^{17}\text{O}_{\text{obs}})/5.8\text{‰}\}$. Therefore, possible range of $f_{\text{S(IV)+O}_3}$ and $f_{\text{zero-}\Delta^{17}\text{O}}$ can be obtained at different
 179 $f_{\text{S(IV)+H}_2\text{O}_2}$ assumptions.

180 In addition, as sulfate with non-zero $\Delta^{17}\text{O}(\text{SO}_4^{2-})$ is produced either via in-cloud reactions or via heterogeneous reactions
 181 or both, Eq. (6) can also be written as follows:

$$182 \Delta^{17}\text{O}_{\text{obs}} = f_{\text{het}} \times \Delta^{17}\text{O}_{\text{het}} + f_{\text{cloud}} \times \Delta^{17}\text{O}_{\text{cloud}} + f_{\text{SO}_2+\text{OH}} \times \Delta^{17}\text{O}_{\text{SO}_2+\text{OH}} + f_{\text{p}} \times \Delta^{17}\text{O}_{\text{p}} \quad (7)$$

183 where f_{het} , f_{cloud} , $f_{\text{SO}_2+\text{OH}}$ and f_{p} respectively represents the fractional contribution of heterogeneous sulfate production, in-cloud
 184 sulfate production, gas-phase sulfate production and primary sulfate to the observed sulfate. $f_{\text{p}} = c(\text{p-SO}_4^{2-})/c(\text{SO}_4^{2-})$, $f_{\text{het}} =$
 185 $\{P_{\text{het}}/(P_{\text{het}}+P_{\text{cloud}}+P_{\text{SO}_2+\text{OH}})\} \times (1-f_{\text{p}})$, $f_{\text{cloud}} = \{P_{\text{cloud}}/(P_{\text{het}}+P_{\text{cloud}}+P_{\text{SO}_2+\text{OH}})\} \times (1-f_{\text{p}})$ and $f_{\text{SO}_2+\text{OH}} = \{P_{\text{SO}_2+\text{OH}}/(P_{\text{het}}+P_{\text{cloud}}+P_{\text{SO}_2+\text{OH}})\} \times$
 186 $(1-f_{\text{p}})$. $\Delta^{17}\text{O}_{\text{het}}$, $\Delta^{17}\text{O}_{\text{cloud}}$, $\Delta^{17}\text{O}_{\text{SO}_2+\text{OH}}$ and $\Delta^{17}\text{O}_{\text{p}}$ respectively represents $\Delta^{17}\text{O}$ of corresponding sulfate produced via above
 187 pathways. Both $\Delta^{17}\text{O}_{\text{SO}_2+\text{OH}}$ and $\Delta^{17}\text{O}_{\text{p}}$ are equal to 0 ‰. $\Delta^{17}\text{O}_{\text{cloud}}$ can be calculated as shown in Eq. (8) as the lifetime of sulfate
 188 produced in clouds will not depend on the specific S(IV) oxidant.

$$189 \Delta^{17}\text{O}_{\text{cloud}} = \frac{6.5\text{‰} \times P_{\text{cloud,S(IV)+O}_3} + 0.7\text{‰} \times P_{\text{cloud,S(IV)+H}_2\text{O}_2}}{P_{\text{cloud}}} \quad (8)$$

190 2.8 Calculation of aerosol liquid water content, aerosol pH and ionic strength (I_s)

191 Aerosol liquid water content, aerosol pH and I_s was calculated by the ISORROPIA II model, which is a thermodynamic
 192 equilibrium model for NH_4^+ - K^+ - Ca^{2+} - Na^+ - Mg^{2+} - SO_4^{2-} - NO_3^- - Cl^- - H_2O aerosols (Fountoukis and Nenes, 2007). The
 193 ISORROPIA II model can solve forward problems in which T , relative humidity and the concentrations of gas + aerosols are
 194 known (e.g., $\text{NH}_3 + \text{NH}_4^+$), and reverse problems in which T , relative humidity and the concentrations of aerosol (but not gas)
 195 species are known. We used the forward method to calculate aerosol liquid water content, aerosol pH and I_s as this method has
 196 been shown to best predict aerosol pH (Hennigan et al., 2015). The aerosol liquid water content, pH and I_s was first calculated
 197 in metastable mode (assuming that bulk aerosol solution is supersaturated), which is consistent with previous studies about
 198 Beijing haze (Liu et al., 2017; Guo et al., 2017). However, the work of Rood et al. (1989) in California, USA suggested that
 199 not all aerosols are in metastable state, even though the fractional occurrence of metastable aerosols increases with increasing
 200 relative humidity in urban sites (roughly following Eq. (9)). We also calculated the aerosol liquid water content, pH and I_s
 201 assuming stable mode (assuming that bulk aerosols crystallize once saturation is exceeded), which is consistent with Wang et
 202 al. (2016). The input of observed inorganic ion concentrations and meteorological parameters are summarized in Table S4.
 203 Since gaseous NH_3 was not measured in our campaign, we used the empirical equation $[\text{NH}_3]/(\text{nmol mol}^{-1}) = 0.34[\text{NO}_x]/(\text{nmol}$
 204 $\text{mol}^{-1}) + 0.63$, derived from observations of Meng et al. (2011) in Beijing winter, to estimate the NH_3 mole fraction. We used
 205 NO_2 mole fraction instead of NO_x as input due to the lack of NO_x observations in our study, which would give a lower end of
 206 NH_3 mole fraction. Given the importance of aerosol liquid water content for reaction rates and the fact that ISORROPIA II
 207 underestimates aerosol liquid water content at low relative humidity (Bian et al., 2014), samples with relative humidity < 40 %

208 are excluded from analysis (Hennigan et al., 2015). This excludes 8 out of the total 34 samples (24 %), with 6 of them in NPD.
 209 A total of 4 samples in NPD and 22 samples in PD were analysed for aerosol liquid water content, aerosol pH and I_s . Due to
 210 that the predicted I_s is high ($I_s > 10$ M, Table S4), which suggests aerosol water is non-ideal, the influence of I_s on reaction rate
 211 constants (Table S3) and effective Henry's law constants (Table S5) is taken into consideration when the influence is known.

$$212 \quad x(\text{metastable}) = \begin{cases} 0, & \Psi < 30 \% \\ -0.024(\Psi/\%)^2 + 4.18\Psi/\% - 89.13, & 30 \% \leq \Psi \leq 80 \% \\ 100 \%, & 80 \% < \Psi \leq 100 \% \end{cases} \quad (9)$$

213 where $x(\text{metastable})$ is the fraction of metastable aerosols to total aerosols in the unit of %.

214 **2.9 Estimate of aqueous concentrations of trace species**

215 The aqueous concentrations of SO_2 , O_3 , H_2O_2 and NO_2 were calculated as described in Table S5. The determination of
 216 in-cloud concentrations of TMIs (here only Fe(III) and Mn(II) (Alexander et al., 2009)) is described below.

217 The concentration of soluble Fe(III) follows Eqs. (10)–(13) (Liu and Millero, 1999):

$$218 \quad \log_{10}([\text{Fe(III)}]/c^\ominus) = \log_{10}(K_{\text{Fe(OH)}_3}^*(c^\ominus)^2) + 3 \log_{10}([\text{H}^+]/c^\ominus) + \log_{10}(1 + \beta_1^*([\text{H}^+]/c^\ominus)^{-1} + \beta_2^*([\text{H}^+]/c^\ominus)^{-2}) \quad (10)$$

219 where

$$220 \quad \log_{10}(K_{\text{Fe(OH)}_3}^*(c^\ominus)^2) = -13.486 - 0.1856(I_s/c^\ominus)^{0.5} + 0.3073(I_s/c^\ominus) + 5254\text{K}/T \quad (11)$$

$$221 \quad \log_{10}(\beta_1^*/(c^\ominus)^2) = 2.517 - 0.8885(I_s/c^\ominus)^{0.5} + 0.2139(I_s/c^\ominus) - 1320\text{K}/T \quad (12)$$

$$222 \quad \log_{10}(\beta_2^*/(c^\ominus)^2) = 0.4511 - 0.3305(I_s/c^\ominus)^{0.5} - 1996\text{K}/T \quad (13)$$

223 and $[\text{Fe(III)}]$ is the aqueous concentration of Fe(III) in unit of M, T is temperature in unit of K, and I_s is ionic strength in unit
 224 of M, $K_{\text{Fe(OH)}_3}^*$ is the solubility product constant of Fe(OH)_3 in the unit of $(\text{mol L}^{-1})^{-2}$, and β_1^* and β_2^* is respectively first-order
 225 and second-order cumulative hydrolysis constants of Fe^{3+} in the unit of $(\text{mol L}^{-1})^2$.

226 Our calculation suggested in-cloud $[\text{Fe(III)}]$ was in the range of 0.6 to 6.1 μM with a mean of (2.6 ± 1.8) μM , which is
 227 similar to the observed values in NCP (Guo et al., 2012; Shen et al., 2012). The concentration of soluble Mn(II) in cloud water
 228 was set to be 1 μM in the present study, which is the general value observed in cloud water in NCP (Guo et al., 2012; Shen et
 229 al., 2012).

230 **2.10 Estimate of sulfate production rate in aerosol water**

231 The reaction rate expressions, rate constants (k) and the influence of I_s on k for sulfate production in aerosol water are
 232 summarized in Table S3. The overall rates for S(IV) oxidation in aerosol water depend not only on chemical reaction rates
 233 (Table S3) but also on mass transport limitations. A standard resistance model was used to estimate effects of mass transport
 234 following the work of Cheng et al. (2016):

$$235 \quad \frac{1}{R_{\text{H,S(IV)+oxi}}} = \frac{1}{R_{\text{S(IV)+oxi}}} + \frac{1}{J_{\text{aq,lim}}} \quad (14)$$

236 where $R_{H, S(IV)+oxi}$ is the overall reaction rate for S(IV) oxidation by a certain oxidant (oxi) such as O_3 , H_2O_2 , NO_2 and O_2 on
 237 acidic microdroplets ($M s^{-1}$), $R_{S(IV)+oxi}$ is the chemical reaction rate ($M s^{-1}$) and $J_{aq, lim}$ is the rate limited by mass transfer from
 238 the gas to the aqueous phase ($M s^{-1}$). Due to the large decrease in the aqueous-phase reaction rate constant for TMI-initiated
 239 S(IV) oxidation by O_2 with increasing I_s (Martin and Hill, 1967) and the high I_s of aerosols (Table S4), combined with the fact
 240 that the rate constant for the S(IV) + O_2 mechanism on acidic microdroplets proposed by Hung and Hoffman (2015) likely
 241 includes the effect of TMIs, we do not directly consider TMI-initiated S(IV) oxidation by O_2 in aerosol water. $R_{S(IV)+oxi}$ was
 242 calculated as described in Table S3. The limiting mass transfer $J_{aq, lim}$ was calculated by Eqs. (15) and (16).

$$243 J_{aq,lim} = \min\{J_{aq}(SO_2), J_{aq}(oxi)\} \quad (15)$$

$$244 J_{aq}(X) = k_{MT}(X) \times [X(aq)] \quad (16)$$

245 where $X = SO_2, O_3, H_2O_2$ or NO_2 and k_{MT} (s^{-1}) is the mass transfer rate coefficient and was calculated as Eq. (17) (Cheng et
 246 al., 2016; Seinfeld and Pandis, 2006):

$$247 k_{MT}(X) = \left[\frac{R_p^2}{3D_g} + \frac{4R_p}{3\alpha v} \right]^{-1} \quad (17)$$

248 where R_p , D_g and v are the same as Eq. (1). The α used in our calculation is respectively 0.11 for SO_2 , 0.23 for H_2O_2 , $2.0 \times 10^{-}$
 249 3 for O_3 and 2.0×10^{-4} for NO_2 (Seinfeld and Pandis, 2006; Jacob, 2000). The term on the left hand side of Eq. (17) is the gas-
 250 phase diffusion limitation while the term on the right hand side of Eq. (17) is the interfacial mass transport limitation. k_{MT} was
 251 limited by interfacial mass transport in our study.

252 The rate of heterogeneous sulfate production by a certain oxidant ($P_{het, S(IV)+oxi}$) in aerosol water can be expressed as:

$$253 P_{het, S(IV)+oxi} = 3600 s h^{-1} \times 96 g mol^{-1} \times R_{H, S(IV)+oxi} \times \frac{L_a}{\rho_w} \quad (18)$$

254 where $P_{het, S(IV)+oxi}$ is in the unit of $\mu g m^{-3} h^{-1}$, $3600 s h^{-1}$ and $96 g mol^{-1}$ is the same as Eq. (1). $R_{H, S(IV)+oxi}$ is in the unit of $M s^{-}$
 255 1 , L_a is aerosol liquid water content in the unit of $mg m^{-3}$, and ρ_w is the density of water ($1 kg L^{-1}$).

256 3 Results and Discussion

257 3.1 Characteristics of haze events in Beijing

258 Figure 1a shows the temporal evolution of concentrations of $PM_{2.5}$ and SO_4^{2-} during our sampling period. The 12h-
 259 averaged $PM_{2.5}$ concentrations ranged from 16 to $323 \mu g m^{-3}$ with a mean of $(141 \pm 88 (1\sigma)) \mu g m^{-3}$. In comparison, the Grade
 260 II of the Chinese National Ambient Air Quality Standard of daily $PM_{2.5}$ is $75 \mu g m^{-3}$. The SO_4^{2-} concentrations varied from
 261 1.5 to $56.4 \mu g m^{-3}$ with a mean of $(21.2 \pm 15.4) \mu g m^{-3}$. As shown in Fig. 1a, SO_4^{2-} concentrations presented a similar temporal
 262 trend as $PM_{2.5}$ concentrations, i.e., increased from a mean of $(3.9 \pm 1.8) \mu g m^{-3}$ in non-polluted days (NPD, $PM_{2.5} < 75 \mu g m^{-3}$)
 263 to $(28.4 \pm 12.5) \mu g m^{-3}$ in polluted days (PD, $PM_{2.5} \geq 75 \mu g m^{-3}$). The fraction of SO_4^{2-} to $PM_{2.5}$ mass concentration ranged
 264 from 8–25 %, and increased from a mean of $(11 \pm 2) \%$ in NPD to $(15 \pm 5) \%$ in PD. The sulfur oxidation ratio (SOR, which

265 equals to SO_4^{2-} molar concentration divided by the sum of SO_4^{2-} and SO_2 molar concentration), a proxy for secondary sulfate
266 formation (Sun et al., 2006), also increased rapidly with $\text{PM}_{2.5}$ levels, from a mean of 0.12 ± 0.04 in NPD to 0.41 ± 0.17 in PD
267 (Fig. 1b).

268 Observed $\Delta^{17}\text{O}(\text{SO}_4^{2-})$ ($\Delta^{17}\text{O}_{\text{obs}}$) ranged from 0.1 ‰ to 1.6 ‰ with a mean of (0.9 ± 0.3) ‰ (Fig. 1b). The highest $\Delta^{17}\text{O}_{\text{obs}}$
269 = 1.6 ‰ occurred during PD of Case II in October 2014 while the lowest $\Delta^{17}\text{O}_{\text{obs}} = 0.1$ ‰ occurred during PD of Case IV in
270 December 2014. $\Delta^{17}\text{O}_{\text{obs}}$ reported here is similar in magnitude to previous observations of $\Delta^{17}\text{O}(\text{SO}_4^{2-})$ in aerosols and rainwater
271 collected in China (Lin et al., 2017; Li et al., 2013) and other mid-latitude sites (Table S6). The overall $\Delta^{17}\text{O}_{\text{obs}}$ levels during
272 our entire sampling time are similar for NPD and PD, being (0.9 ± 0.1) ‰ and (0.9 ± 0.4) ‰, respectively. However, the NPD
273 to PD difference of $\Delta^{17}\text{O}_{\text{obs}}$ can be case-dependent. For Case I and II in October 2014, $\Delta^{17}\text{O}_{\text{obs}}$ increased from NPD to PD,
274 while the opposite trend was observed for Case III to V in November 2014 to January 2015 (Fig. 1b). These $\Delta^{17}\text{O}_{\text{obs}}$ variations
275 are generally similar to variability in mole fractions of observed O_3 and calculated H_2O_2 (Fig. 1c), which is consistent with the
276 fact that O_3 and H_2O_2 are the sole sources of non-zero $\Delta^{17}\text{O}(\text{SO}_4^{2-})$ (Table 1).

277 3.2 Direct estimate of sulfate formation pathways based on $\Delta^{17}\text{O}_{\text{obs}}$

278 Figure 2 shows the calculated possible fractional contributions of each formation pathway ($f_{\text{S(IV)+H}_2\text{O}_2}$, $f_{\text{S(IV)+O}_3}$, and $f_{\text{zero-}}$
279 $\Delta^{17}\text{O}$) for each sample using Eq. (6). On average over all samples collected, $f_{\text{S(IV)+O}_3} = 4\text{--}13\%$, $f_{\text{S(IV)+H}_2\text{O}_2} = 0\text{--}88\%$, and $f_{\text{zero-}}$
280 $\Delta^{17}\text{O} = 8\text{--}87\%$. For samples during PD of Case IV in December 2014 with the three lowest $\Delta^{17}\text{O}_{\text{obs}}$ values (Fig. 1b), $f_{\text{zero-}}$
281 $\Delta^{17}\text{O}$ was respectively in the range of 57–95 %, 86–98 % and 57–95 %, corresponding to $f_{\text{S(IV)+H}_2\text{O}_2}$ being in the range of 0–43 %,
282 0–14 % and 0–43 % respectively, which clearly suggests zero- $\Delta^{17}\text{O}$ pathways dominated sulfate formation during PD of Case
283 IV. However, for other samples, the maximum possible $f_{\text{S(IV)+H}_2\text{O}_2}$ ranged from 71 % to 100 % with a mean of (93 ± 7) % while
284 the maximum possible $f_{\text{zero-}}$ $\Delta^{17}\text{O}$ was 75 % to 92 % with a mean of (86 ± 4) %, implying that sulfate formation during these
285 sampling periods were dominated by H_2O_2 oxidation and/or zero- $\Delta^{17}\text{O}$ pathways.

286 3.3 Chemical kinetic calculations with the constraint of $\Delta^{17}\text{O}_{\text{obs}}$

287 The good correlation between relative humidity and SOR in Fig. 3a ($r = 0.76$, $p < 0.01$) suggests heterogeneous reactions
288 played an important role in sulfate formation. Our local atmospheric conditions-based calculations show that overall
289 heterogeneous sulfate production (P_{het} , see Sect. 2.3) presented similar trends with SO_4^{2-} concentrations except for Case II
290 (Fig. 3b) and increased from a mean of $(0.6 \pm 0.3) \mu\text{g m}^{-3} \text{h}^{-1}$ in NPD to $(2.0 \pm 1.1) \mu\text{g m}^{-3} \text{h}^{-1}$ in PD during our entire sampling
291 period. In comparison, Cheng et al. (2016) reported that the missing sulfate production rate required to explain the observed
292 sulfate concentration is around $0.07 \mu\text{g m}^{-3} \text{h}^{-1}$ when $\text{PM}_{2.5} < 50 \mu\text{g m}^{-3}$ and around $4 \mu\text{g m}^{-3} \text{h}^{-1}$ when $\text{PM}_{2.5} > 400 \mu\text{g m}^{-3}$
293 during 2013 Beijing haze. We also calculated the contribution from primary sulfate and performed chemical kinetic
294 calculations including SO_2 oxidation by OH in the gas-phase and in-cloud sulfate production (Fig. 4 and Table 2, see Sect.

295 2.4–2.6) to estimate the relative importance of heterogeneous sulfate production in our sampling period. Heterogeneous
296 reactions were found to contribute 41–54 % to total sulfate formation during PD of Case I and III–V, with a mean of (48 ± 5) %
297 (Fig. 4). This is consistent with Zheng et al. (2015a) who modelled that about half of the observed sulfate was from
298 heterogeneous reactions during 2013 Beijing haze. In contrast, we found that during PD of Case II in October 2014,
299 heterogeneous sulfate production only accounted for 23 % of total sulfate production while in-cloud sulfate production
300 predominated total sulfate production with an estimated fraction of 68 %. The predominant role of in-cloud sulfate production
301 in PD of Case II was supported by the relative high cloud liquid water content during this time period (Fig. 5a). Our local
302 atmospheric conditions-based calculations also suggest the in-cloud sulfate production was dominated by H_2O_2 oxidation
303 throughout our sampling period (Fig. 5b), which is consistent with previous findings that H_2O_2 oxidation is the most important
304 in-cloud sulfate production pathway globally (Alexander et al., 2012) and in NCP (Shen et al., 2012). In addition, the $\Delta^{17}\text{O}$ of
305 sulfate produced in clouds ($\Delta^{17}\text{O}_{\text{cloud}}$) was estimated to range from 0.5 ‰ to 0.8 ‰ with a mean of (0.6 ± 0.1) ‰ during our
306 sampling period and showed similar variations with $\Delta^{17}\text{O}_{\text{obs}}$ (Fig. 5c). The mean value of $\Delta^{17}\text{O}_{\text{cloud}}$ calculated here is close to
307 $\Delta^{17}\text{O}(\text{SO}_4^{2-})$ in rainwater observed in central China (0.53 ± 0.19) ‰ (Li et al., 2013) and at Baton Rouge, USA (0.62 ± 0.32) ‰
308 (Jenkins and Bao, 2006). In addition, by using Eq. (7), the $\Delta^{17}\text{O}$ of sulfate produced via heterogeneous reactions ($\Delta^{17}\text{O}_{\text{het}}$) was
309 calculated to be respectively 1.8 ‰, 3.1 ‰, 1.4 ‰, 0.1 ‰ and 0.8 ‰ for PD of Case I–V. Since $\Delta^{17}\text{O}(\text{SO}_4^{2-})$ produced via
310 H_2O_2 oxidation is 0.7 ‰, smaller than $\Delta^{17}\text{O}_{\text{het}}$ in Case I–III and V, O_3 oxidation must contribute to heterogeneous sulfate
311 production.

312 To explore the specific mechanisms of heterogeneous oxidation of SO_2 , we calculated aerosol parameters such as aerosol
313 liquid water content, pH and ionic strength (I_s) by using the ISORROPIA II thermodynamic model (Fountoukis and Nenes,
314 2007) (Fig.6, see Sect. 2.8). It was found that the assumptions about aerosol thermodynamic state (salts crystallize once
315 saturation is exceeded, termed as “stable state” or aerosol solution is supersaturated, termed as “metastable state”) significantly
316 influence the calculated aerosol pH, but have little impact on the calculated aerosol liquid water content and I_s (Fig. 6).
317 Calculated aerosol liquid water content increased with $\text{PM}_{2.5}$ concentrations, from (5.3 ± 7.4) $\mu\text{g m}^{-3}$ in NPD to (63.5 ± 54.6) μg
318 m^{-3} in PD when assuming stable state and from (9.6 ± 6.0) $\mu\text{g m}^{-3}$ in NPD to (84.2 ± 49.2) $\mu\text{g m}^{-3}$ in PD when assuming
319 metastable state (Fig. 6a). Calculated I_s was similar for stable and metastable assumptions, ranging from 11.3 to 51.6 M (Fig.
320 6b). The high I_s suggested aerosol water was non-ideal and thus the influence of I_s on reaction rate constants (Table S3) and
321 effective Henry’s law constants (Table S5) was taken into consideration when the influence is known. The bulk aerosol pH
322 predicted in stable state was in the range of 7.5 to 7.8 with a mean of 7.6 ± 0.1 , consistent with bulk aerosol pH = 7.63 ± 0.03
323 calculations during a haze event in Beijing 2015 predicted by Wang et al. (2016). The bulk aerosol pH calculated assuming
324 metastable state was in the range of 3.4 to 7.6 with a mean of 4.7 ± 1.1 , consistent with the mean value of 4.2 calculated in
325 metastable aerosol assumption during severe haze in Beijing 2015–2016 by Liu et al. (2017). The calculated aerosol pH

326 assuming metastable state decreased with increasing $PM_{2.5}$ levels, from a mean of 6.5 ± 1.3 in NPD to 4.4 ± 0.6 in PD, while that
327 assuming stable state shows no relationship with $PM_{2.5}$ concentrations (Fig. 6c). Our measured pH of filtrate ranged from 4.6
328 to 8.2 with a mean of 5.7 ± 1.0 , similar to pH of filtrate from $PM_{2.5}$ in Beijing reported by Wang et al. (2005). The measured
329 pH of filtrate shows similar trends with bulk aerosol pH calculated assuming metastable state (Fig. 6c), with a mean value
330 6.9 ± 0.7 in NPD and 5.1 ± 0.6 in PD, which suggests that bulk aerosols are in metastable state with moderate acidity in PD. This
331 is also consistent with our estimate that most aerosols are in metastable with a fraction of $(74\pm 17)\%$ in PD by using Eq. (9)
332 and our cognition that the mixture of major acidic aerosols with minor neutral aerosols would lead to the bulk being acidic.
333 However, as the effective Henry's law constant of SO_2 at $pH = 7.6$ (stable state) can be 3 orders magnitude higher than that at
334 $pH = 4.4$ (metastable state in PD) rendering even a small fraction of aerosol at this high pH value being potentially significant
335 active sites for heterogeneous sulfate production during PD.

336 The main heterogeneous sulfate formation pathways considered include S(IV) oxidation by H_2O_2 , O_3 , NO_2 and O_2 on
337 acidic microdroplets as proposed by Hung and Hoffmann (2015). Other sulfate formation pathways such as S(IV) oxidation
338 by NO_3 radical, methyl-hydrogenperoxide (MHP), peroxyacetic acid (PAA), and hypohalous acids in aerosol water (Feingold
339 et al., 2002; Walcek and Taylor, 1986; Chen et al., 2017) is thought to be negligible during haze in NCP (Cheng et al., 2016),
340 and thus is not considered here. We estimate the relative importance of these heterogeneous sulfate formation pathways as
341 follows. First, the heterogeneous sulfate production rate via S(IV) oxidation by H_2O_2 ($P_{het, S(IV)+H_2O_2}$) was calculated with the
342 influence of I_s being considered, which has been determined at high I_s in laboratories (Table S3 and S5). Then, the fractional
343 contribution of H_2O_2 oxidation ($f_{het, S(IV)+H_2O_2}$) to overall heterogeneous sulfate production (P_{het}) calculated using apparent γ
344 (see Sect. 2.3) was estimated. Large uncertainties exist in the influence of I_s on the reaction rate constant of S(IV) oxidation
345 by O_3 in aerosol water (Table S3), renders the estimate of its fractional contribution ($f_{het, S(IV)+O_3}$) to P_{het} from purely chemical
346 kinetic calculations uncertain. Instead, $f_{het, S(IV)+O_3}$ was estimated using our calculated $f_{het, S(IV)+H_2O_2}$ and $\Delta^{17}O_{het}$ values, on the
347 basis that $\Delta^{17}O(SO_4^{2-}) > 0\%$ originates solely from H_2O_2 and O_3 oxidation. Then zero- $\Delta^{17}O$ pathways such as S(IV) oxidation
348 by NO_2 and by O_2 was estimated to be the remaining part ($f_{het, zero-\Delta^{17}O}$). At last, the potential importance of S(IV) oxidation by
349 NO_2 and by O_2 is discussed.

350 Calculations show that $f_{het, S(IV)+H_2O_2}$ was 4–6 % with a mean of $(5\pm 1)\%$ under stable aerosol assumptions, and 8–19 %
351 with a mean of $(13\pm 4)\%$ under metastable state assumptions for PD of all the cases. $f_{het, S(IV)+O_3}$ was calculated to be 2–47 %
352 with a mean of $(22\pm 17)\%$ in stable state assumption and 0–47 % with a mean of $(21\pm 18)\%$ in metastable state assumption.
353 Correspondingly, $f_{het, zero-\Delta^{17}O}$ was the remaining 73 % (47–94 %) in stable assumption, or 66 % (42–81 %) in metastable
354 assumption for PD of all the cases (Fig. 7). Excluding PD of Case II, in which sulfate formation was predominated by in-cloud
355 reactions, our local atmospheric conditions-based calculations suggest zero- $\Delta^{17}O$ pathways such as S(IV) oxidation by NO_2
356 and/or by O_2 are important for sulfate formation during Beijing haze.

357 Cheng et al. (2016) suggested that S(IV) oxidation by NO₂ in aerosol water could largely account for the missing sulfate
358 source in 2013 Beijing haze. In their study, the calculated mean aerosol pH is 5.8, while influence of I_s was not taken into
359 account due to the lack of relevant experimental data. The calculated $P_{\text{het, S(IV)+NO}_2}$ is highly sensitive to aerosol pH. In our
360 study, when aerosol pH decreased from 7.6 ± 0.1 assuming stable state to 4.7 ± 1.1 assuming metastable state, mean $P_{\text{het, S(IV)+NO}_2}$
361 decreased from $(6.5 \pm 7.7) \mu\text{g m}^{-3} \text{h}^{-1}$ to $(0.01 \pm 0.02) \mu\text{g m}^{-3} \text{h}^{-1}$ for PD of all the cases (Fig. 7). The former is much larger than
362 our estimate of overall heterogeneous production rate, $P_{\text{het}} = (2.0 \pm 1.1) \mu\text{g m}^{-3} \text{h}^{-1}$, while the latter is too small. Moreover, the
363 influence of I_s was not considered, which is expected to increase the reaction rate constant of S(IV) oxidation by NO₂ (Cheng
364 et al., 2016). The treatment of aerosols as a bulk quantity, assuming that all aerosols are either in stable or metastable state, or
365 that all aerosol particles have the same pH, may lead to errors in calculating heterogeneous sulfate production rates. As stated
366 in Sect. 2.8, not all aerosols are in metastable state, even though the fractional occurrence of metastable aerosols increases with
367 increasing relative humidity (Rood et al., 1989). Fig. 8a shows that the fraction of metastable aerosols to total aerosols,
368 estimated by using Eq. (9), increases with PM_{2.5} levels. However, when assuming a combination of stable and metastable state
369 aerosol as shown in Eq. (9), $P_{\text{het, S(IV)+NO}_2}$ increases with PM_{2.5} levels and reaches $(0.9 \pm 0.7) \mu\text{g m}^{-3} \text{h}^{-1}$ during PD of all the
370 cases (Fig. 8b), much higher than $P_{\text{het, S(IV)+NO}_2} = (0.01 \pm 0.02) \mu\text{g m}^{-3} \text{h}^{-1}$ under sole metastable aerosol assumption. This estimate
371 suggests that even though the majority of aerosols may be in metastable state during PD ($74 \pm 17\%$ in our calculation), the
372 high pH of the minority of aerosols in stable state could render S(IV) oxidation by NO₂ a potentially significant pathway for
373 heterogeneous sulfate production.

374 Since $P_{\text{het, S(IV)+NO}_2}$ using calculated aerosol pH assuming metastable state was two orders of magnitude lower than P_{het}
375 during PD, we further examined S(IV) oxidation by O₂ on acidic microdroplets under the metastable state assumption. A
376 laboratory study suggested that SO₂ oxidation by O₂ on acidic microdroplets has a large aqueous-phase reaction rate constant
377 of $1.5 \times 10^6 [\text{S(IV)}] (\text{M s}^{-1})$ at $\text{pH} \leq 3$, a pH range much lower than our calculated pH values. The rate constant was shown to
378 decrease with increasing pH, however, no values of the rate constant at $\text{pH} > 3$ was reported (Hung and Hoffmann, 2015).
379 Figure 7b shows heterogenous sulfate production rate via S(IV) oxidation by O₂ on acidic microdroplets ($P_{\text{het, S(IV)+O}_2}$) with
380 aerosol liquid water content calculated assuming metastable state and the aqueous-phase rate constant for $\text{pH} \leq 3$ being used,
381 even though the calculated aerosol pH is > 3 . The estimated $P_{\text{het, S(IV)+O}_2}$ is 1.5×10^3 to $1.3 \times 10^5 \mu\text{g m}^{-3} \text{h}^{-1}$ with a mean of 2.5×10^4
382 $\mu\text{g m}^{-3} \text{h}^{-1}$ during PD of all cases, which is four order of magnitude larger than P_{het} . This value should be an overestimate due
383 to our calculated bulk aerosol pH predicted in metastable state being 4.4 ± 0.6 during PD and the experimental results of He et
384 al. (2014) and Wang et al. (2016) suggests O₂ oxidation pathway is negligible at higher pH conditions (e.g., on CaO and in
385 NH₄⁺ solution). However, some fraction of aerosols may have $\text{pH} \leq 3$ due to the Kelvin effect (Hung and Hoffmann, 2015),
386 rendering S(IV) oxidation by O₂ on acidic microdroplets a potentially important pathway for heterogeneous sulfate production
387 even if it may occur on only a small fraction of the ambient aerosol.

388 4 Conclusions

389 Our study suggests that both in-cloud reactions and heterogeneous reactions can dominate sulfate formation during
390 Beijing haze, with the fractional contribution of $f_{\text{cloud}} = 68\%$ in Case II and $f_{\text{het}} = (48 \pm 5)\%$ in Case I and III–V. The $\Delta^{17}\text{O}$ -
391 constrained calculation shows that the heterogeneous sulfate production during haze events in our observation was mainly (66
392 to 73 % on average) from reactions that result in sulfate with $\Delta^{17}\text{O} = 0\%$, e.g., S(IV) oxidation by NO_2 and/or by O_2 . S(IV)
393 oxidation by H_2O_2 and O_3 accounted for the rest (27 to 34 %) of heterogeneous sulfate production. However, given the large
394 difference in predicted aerosol pH assuming metastable aerosol state and stable aerosol state ($\text{pH} = 7.6 \pm 0.1$ and 4.7 ± 1.1 ,
395 respectively) and the strong dependence of SO_2 oxidation on aerosol pH, we cannot quantify the relative importance of these
396 two pathways for heterogeneous sulfate production. S(IV) + NO_2 can be the dominant pathway when aerosols are in stable
397 state with $\text{pH} = 7.6 \pm 0.1$, while S(IV) + O_2 can take over providing that highly acidic aerosols ($\text{pH} \leq 3$) exist. To distinguish
398 which of these two mechanisms is more important for sulfate formation during Beijing haze, the heterogeneity of aerosol state
399 and pH should be considered in future studies.

400 Supplementary Materials

401 **Table S1.** Reaction rate expression and constant for SO_2 oxidation by OH in the gas-phase.

402 **Table S2.** The daytime average OH concentration.

403 **Table S3.** Aqueous-phase reaction rate expressions, rate constants (k) and influence of ionic strength (I_s) on k for sulfate
404 production in aerosol and cloud water.

405 **Table S4.** Summary for the input and output of ISORROPIA II model.

406 **Table S5.** Calculations of aqueous-phase concentrations, equilibrium constants and influence of ionic strength.

407 **Table S6.** Observed $\Delta^{17}\text{O}(\text{SO}_4^{2-})$ in aerosols or rainwater in mid-latitude areas.

408 Data availability

409 All data needed to draw the conclusions in the present study are shown in this paper and/or the Supplementary Materials.
410 For additional data related to this study, please contact the corresponding author (zqxie@ustc.edu.cn).

411 Author contributions

412 Z.Q.X. conceived the study. P.Z.H. conducted oxygen isotope measurements supervised by B.A. and L.G.. P.Z.H., X.Y.C.,
413 S.D.F., H.C.Z., H. K. performed the field experiments and aerosol chemical composition measurements. P.Z.H., B.A., Z.Q.X.,
414 L.G., H.S. and Y.F.C. interpreted the data. H.S., Y.F.C. and G.J.Z. involved the discussion of oxidation pathway calculation.

415 C.L. contributed to the field observation support. P.Z.H. wrote the manuscript with B.A., Z.Q.X. and L.G. inputs. All authors
416 involved the discussion and revision.

417 **Competing interests**

418 The authors declare no competing interests.

419 **Acknowledgments**

420 We thank A. J. Schauer and Q. J. Chen at the University of Washington for help with isotope ratio measurements. Z. Q.
421 Xie acknowledges support from National Key Project of MOST (2016YFC0203302), NSFC (91544013), the Key Project of
422 CAS (KJZD-EW-TZ-G06-01) and the Atmospheric Pollution Control of the Prime Minister (DQGG0104). B. Alexander
423 acknowledges support from NSF AGS 1644998. H. Su acknowledges support from National Key Project of MOST
424 (2017YFC0210104) and NSFC (91644218).

425 **References**

- 426 Alexander, B., Park, R. J., Jacob, D. J., Li, Q., Yantosca, R. M., Savarino, J., Lee, C., and Thiemens, M.: Sulfate formation in
427 sea-salt aerosols: Constraints from oxygen isotopes, *J. Geophys. Res.*, 110, D10307, 2005.
- 428 Alexander, B., Park, R. J., Jacob, D. J., and Gong, S.: Transition metal-catalyzed oxidation of atmospheric sulfur: Global
429 implications for the sulfur budget, *J. Geophys. Res.*, 114, D02309, 2009.
- 430 Alexander, B., Allman, D., Amos, H., Fairlie, T., Dachs, J., Hegg, D. A., and Sletten, R. S.: Isotopic constraints on the
431 formation pathways of sulfate aerosol in the marine boundary layer of the subtropical northeast Atlantic Ocean, *J.*
432 *Geophys. Res.*, 117, D06304, 2012.
- 433 Bao, H., Thiemens, M. H., Farquhar, J., Campbell, D. A., Lee, C. C.-W., Heine, K., and Loope, D. B.: Anomalous ^{17}O
434 compositions in massive sulphate deposits on the Earth, *Nature*, 406, 176-178, 2000.
- 435 Bian, Y., Zhao, C., Ma, N., Chen, J., and Xu, W.: A study of aerosol liquid water content based on hygroscopicity
436 measurements at high relative humidity in the North China Plain, *Atmos. Chem. Phys.*, 14, 6417-6426, 2014.
- 437 Brook, R. D., Rajagopalan, S., Pope, C. A., Brook, J. R., Bhatnagar, A., Diez-Roux, A. V., Holguin, F., Hong, Y., Luepker, R.
438 V., and Mittleman, M. A.: Particulate matter air pollution and cardiovascular disease an update to the scientific statement
439 from the American Heart Association, *Circulation*, 121, 2331-2378, 2010.
- 440 Calhoun, J. A., Bates, T. S., and Charlson, R. J.: Sulfur isotope measurements of submicrometer sulfate aerosol particles over
441 the Pacific Ocean, *Geophys. Res. Lett.*, 18, 1877-1880, 1991.

442 Chen, Q., Geng, L., Schmidt, J. A., Xie, Z., Kang, H., Dachs, J., Cole-Dai, J., Schauer, A. J., Camp, M. G., and Alexander, B.:
443 Isotopic constraints on the role of hypohalous acids in sulfate aerosol formation in the remote marine boundary layer,
444 *Atmos. Chem. Phys.*, 16, 11433-11450, 2016.

445 Chen, Q., Schmidt, J. A., Shah, V., Jaeglé, L., Sherwen, T., and Alexander, B.: Sulfate production by reactive bromine:
446 Implications for the global sulfur and reactive bromine budgets, *Geophys. Res. Lett.*, 2017.

447 Cheng, Y., Zheng, G., Wei, C., Mu, Q., Zheng, B., Wang, Z., Gao, M., Zhang, Q., He, K., and Carmichael, G.: Reactive
448 nitrogen chemistry in aerosol water as a source of sulfate during haze events in China, *Sci. Adv.*, 2, e1601530, 2016.

449 Cheng, Z., Jiang, J., Fajardo, O., Wang, S., and Hao, J.: Characteristics and health impacts of particulate matter pollution in
450 China (2001–2011), *Atmos. Environ.*, 65, 186-194, 2013.

451 Clifton, C. L., Altstein, N., and Huie, R. E.: Rate constant for the reaction of nitrogen dioxide with sulfur (IV) over the pH
452 range 5.3-13, *Environ. Sci. Technol.*, 22, 586-589, 1988.

453 Dubey, M. K., Mohrschladt, R., Donahue, N. M., and Anderson, J. G.: Isotope specific kinetics of hydroxyl radical (OH) with
454 water (H₂O): Testing models of reactivity and atmospheric fractionation, *J. Phys. Chem. A*, 101, 1494-1500, 1997.

455 Faloon, I.: Sulfur processing in the marine atmospheric boundary layer: A review and critical assessment of modeling
456 uncertainties, *Atmos. Environ.*, 43, 2841-2854, 2009.

457 Feingold, G., Frost, G. J., and Ravishankara, A.: Role of NO₃ in sulfate production in the wintertime northern latitudes, *J.*
458 *Geophys. Res.*, 107, 2002.

459 Fountoukis, C., and Nenes, A.: ISORROPIA II: a computationally efficient thermodynamic equilibrium model for K⁺-Ca²⁺-
460 Mg²⁺-NH₄⁺-Na⁺-SO₄²⁻-NO₃⁻-Cl⁻-H₂O aerosols, *Atmos. Chem. Phys.*, 7, 4639-4659, 2007.

461 Fu, A.: Study on peroxides concentration and its influencing factors in the urban atmosphere, master of engineering, College
462 of Environmental and Resource Sciences, Zhejiang University, Hangzhou, China, 56 pp., 2014.(in Chinese)

463 Geng, L., Schauer, A. J., Kunasek, S. A., Sofen, E. D., Erbland, J., Savarino, J., Allman, D. J., Sletten, R. S., and Alexander,
464 B.: Analysis of oxygen-17 excess of nitrate and sulfate at sub-micromole levels using the pyrolysis method, *Rapid*
465 *Commun. Mass Spectrom.*, 27, 2411-2419, 2013.

466 Guo, H., Weber, R. J., and Nenes, A.: High levels of ammonia do not raise fine particle pH sufficiently to yield nitrogen oxide-
467 dominated sulfate production, *Sci. Rep.*, 7, 12109, 2017.

468 Guo, J., Wang, Y., Shen, X., Wang, Z., Lee, T., Wang, X., Li, P., Sun, M., Collett, J. L., and Wang, W.: Characterization of
469 cloud water chemistry at Mount Tai, China: Seasonal variation, anthropogenic impact, and cloud processing, *Atmos.*
470 *Environ.*, 60, 467-476, 2012.

471 Guo, S., Hu, M., Zamora, M. L., Peng, J., Shang, D., Zheng, J., Du, Z., Wu, Z., Shao, M., and Zeng, L.: Elucidating severe
472 urban haze formation in China, *P. Natl. Acad. Sci. USA*, 111, 17373-17378, 2014.

473 Harris, E., Sinha, B., van Pinxteren, D., Tilgner, A., Fomba, K. W., Schneider, J., Roth, A., Gnauk, T., Fahlbusch, B., Mertes,
474 S., Lee, T., Collett, J., Foley, S., Borrmann, S., Hoppe, P., and Herrmann, H.: Enhanced Role of Transition Metal Ion
475 Catalysis During In-Cloud Oxidation of SO₂, *Science*, 340, 727-730, 2013.

476 He, H., Wang, Y., Ma, Q., Ma, J., Chu, B., Ji, D., Tang, G., Liu, C., Zhang, H., and Hao, J.: Mineral dust and NO_x promote
477 the conversion of SO₂ to sulfate in heavy pollution days, *Sci. Rep.*, 4, 4172, 2014.

478 Hennigan, C., Izumi, J., Sullivan, A., Weber, R., and Nenes, A.: A critical evaluation of proxy methods used to estimate the
479 acidity of atmospheric particles, *Atmos. Chem. Phys.*, 15, 2775-2790, 2015.

480 Hoffmann, M. R., and Calvert, J. G.: Chemical Transformation Modules for Eulerian Acid Deposition Models: Volume II, the
481 Aqueous-phase Chemistry, Atmospheric Sciences Research Laboratory, Office of Research and Development, US
482 Environmental Protection Agency, 1985.

483 Holt, B., Kumar, R., and Cunningham, P.: Oxygen-18 study of the aqueous-phase oxidation of sulfur dioxide, *Atmos. Environ.*,
484 15, 557-566, 1981.

485 Hung, H.-M., and Hoffmann, M. R.: Oxidation of gas-Phase SO₂ on the surfaces of acidic microdroplets: Implications for
486 sulfate and sulfate radical anion formation in the atmospheric liquid phase, *Environ. Sci. Technol.*, 49, 13768-13776,
487 2015.

488 Ibusuki, T., and Takeuchi, K.: Sulfur dioxide oxidation by oxygen catalyzed by mixtures of manganese (II) and iron (III) in
489 aqueous solutions at environmental reaction conditions, *Atmos. Environ.*, 21, 1555-1560, 1987.

490 Ishino, S., Hattori, S., Savarino, J., Jourdain, B., Preunkert, S., Legrand, M., Caillon, N., Barbero, A., Kuribayashi, K., and
491 Yoshida, N.: Seasonal variations of triple oxygen isotopic compositions of atmospheric sulfate, nitrate, and ozone at
492 Dumont d'Urville, coastal Antarctica, *Atmos. Chem. Phys.*, 17, 3713-3727, 2017.

493 Jacob, D. J.: Heterogeneous chemistry and tropospheric ozone, *Atmos. Environ.*, 34, 2131-2159, 2000.

494 Jenkins, K. A., and Bao, H.: Multiple oxygen and sulfur isotope compositions of atmospheric sulfate in Baton Rouge, LA,
495 USA, *Atmos. Environ.*, 40, 4528-4537, 2006.

496 Jiang, J., Zhou, W., Cheng, Z., Wang, S., He, K., and Hao, J.: Particulate matter distributions in China during a winter period
497 with frequent pollution episodes (January 2013), *Aerosol Air Qual. Res.*, 15, 494-503, 2015.

498 Lee, C. W., Savarino, J., Cachier, H., and Thiemens, M.: Sulfur (³²S, ³³S, ³⁴S, ³⁶S) and oxygen (¹⁶O, ¹⁷O, ¹⁸O) isotopic ratios
499 of primary sulfate produced from combustion processes, *Tellus B*, 54, 193-200, 2002.

500 Lee, Y. N., and Schwartz, S. E.: Kinetics of oxidation of aqueous sulfur (IV) by nitrogen dioxide, in: Kinetics of oxidation of
501 aqueous sulfur (IV) by nitrogen dioxide, Precipitation scavenging, dry Deposition and resuspension, California, 1982,
502 453-470, 1983.

503 Legrand, M., Hammer, C., De Angelis, M., Savarino, J., Delmas, R., Clausen, H., and Johnsen, S. J.: Sulfur-containing species
504 (methanesulfonate and SO₄) over the last climatic cycle in the Greenland Ice Core Project (central Greenland) ice core,
505 J. Geophys. Res., 102, 26663-26679, 1997.

506 Legrand, M., and Mayewski, P.: Glaciochemistry of polar ice cores: A review, Rev. Geophys., 35, 219-243, 1997.

507 Li, L., Chen, Z., Zhang, Y., Zhu, T., Li, J., and Ding, J.: Kinetics and mechanism of heterogeneous oxidation of sulfur dioxide
508 by ozone on surface of calcium carbonate, Atmos. Chem. Phys., 6, 2453-2464, 2006.

509 Li, X., Bao, H., Gan, Y., Zhou, A., and Liu, Y.: Multiple oxygen and sulfur isotope compositions of secondary atmospheric
510 sulfate in a mega-city in central China, Atmos. Environ., 81, 591-599, 2013.

511 Lin, M., Biglari, S., Zhang, Z., Crocker, D., Tao, J., Su, B., Liu, L., and Thiemens, M. H.: Vertically uniform formation
512 pathways of tropospheric sulfate aerosols in East China detected from triple stable oxygen and radiogenic sulfur isotopes,
513 Geophys. Res. Lett., 2017.

514 Liu, M., Song, Y., Zhou, T., Xu, Z., Yan, C., Zheng, M., Wu, Z., Hu, M., Wu, Y., and Zhu, T.: Fine Particle pH during Severe
515 Haze Episodes in Northern China, Geophys. Res. Lett., 2017.

516 Liu, X., and Millero, F. J.: The solubility of iron hydroxide in sodium chloride solutions, Geochim. Cosmochim. Acta, 63,
517 3487-3497, 1999.

518 Luz, B., and Barkan, E.: The isotopic ratios ¹⁷O/¹⁶O and ¹⁸O/¹⁶O in molecular oxygen and their significance in biogeochemistry,
519 Geochim. Cosmochim. Acta, 69, 1099-1110, 2005.

520 Martin, L. R., and Hill, M. W.: The iron catalyzed oxidation of sulfur: Reconciliation of the literature rates, Atmos. Environ.,
521 21, 1487-1490, 1967.

522 Matsuhisa, Y., Goldsmith, J. R., and Clayton, R. N.: Mechanisms of hydrothermal crystallization of quartz at 250 °C and 15
523 kbar, Geochim. Cosmochim. Acta, 42, 173-182, 1978.

524 McArdle, J. V., and Hoffmann, M. R.: Kinetics and mechanism of the oxidation of aquated sulfur dioxide by hydrogen peroxide
525 at low pH, J. Phys. Chem., 87, 5425-5429, 1983.

526 Meng, Z., Lin, W., Jiang, X., Yan, P., Wang, Y., Zhang, Y., Jia, X., and Yu, X.: Characteristics of atmospheric ammonia over
527 Beijing, China, Atmos. Chem. Phys., 11, 6139-6151, 2011.

528 Rood, M., Shaw, M., Larson, T., and Covert, D.: Ubiquitous nature of ambient metastable aerosol, Nature, 337, 537-539, 1989.

529 Savarino, J., and Thiemens, M. H.: Analytical procedure to determine both δ¹⁸O and δ¹⁷O of H₂O₂ in natural water and first
530 measurements, Atmos. Environ., 33, 3683-3690, 1999.

531 Savarino, J., Lee, C. C., and Thiemens, M. H.: Laboratory oxygen isotopic study of sulfur (IV) oxidation: Origin of the mass-
532 independent oxygen isotopic anomaly in atmospheric sulfates and sulfate mineral deposits on Earth, J. Geophys. Res.,
533 105, 29079-29088, 2000.

534 Savarino, J., Alexander, B., Darmohusodo, V., and Thiemens, M. H.: Sulfur and oxygen isotope analysis of sulfate at
535 micromole levels using a pyrolysis technique in a continuous flow system, *Anal. Chem.*, 73, 4457-4462, 2001.

536 Seinfeld, J. H., and Pandis, S. N.: *Atmospheric chemistry and physics: From air pollution to climate change*, John Wiley &
537 Sons, New Jersey, 2006.

538 Shen, C. H., and Rochelle, G. T.: Nitrogen dioxide absorption and sulfite oxidation in aqueous sulfite, *Environ. Sci. Technol.*,
539 32, 1994-2003, 1998.

540 Shen, X., Lee, T., Guo, J., Wang, X., Li, P., Xu, P., Wang, Y., Ren, Y., Wang, W., and Wang, T.: Aqueous phase sulfate
541 production in clouds in eastern China, *Atmos. Environ.*, 62, 502-511, 2012.

542 Sofen, E., Alexander, B., Steig, E., Thiemens, M., Kunasek, S., Amos, H., Schauer, A., Hastings, M., Bautista, J., and Jackson,
543 T.: WAIS Divide ice core suggests sustained changes in the atmospheric formation pathways of sulfate and nitrate since
544 the 19th century in the extratropical Southern Hemisphere, *Atmos. Chem. Phys.*, 14, 5749-5769, 2014.

545 Sun, Y., Zhuang, G., Tang, A., Wang, Y., and An, Z.: Chemical characteristics of PM_{2.5} and PM₁₀ in haze-fog episodes in
546 Beijing, *Environ. Sci. Technol.*, 40, 3148-3155, 2006.

547 Vicars, W. C., and Savarino, J.: Quantitative constraints on the $\Delta^{17}\text{O}$ signature of surface ozone: Ambient
548 measurements from 50 °N to 50 °S using the nitrite-coated filter technique, *Geochim. Cosmochim. Acta*, 135, 270-287,
549 2014.

550 Walcek, C. J., and Taylor, G. R.: A theoretical method for computing vertical distributions of acidity and sulfate production
551 within cumulus clouds, *J. Atmos. Sci.*, 43, 339-355, 1986.

552 Wang, G., Zhang, R., Gomez, M. E., Yang, L., Zamora, M. L., Hu, M., Lin, Y., Peng, J., Guo, S., and Meng, J.: Persistent
553 sulfate formation from London Fog to Chinese haze, *P. Natl. Acad. Sci. USA*, 113, 13630-13635, 2016.

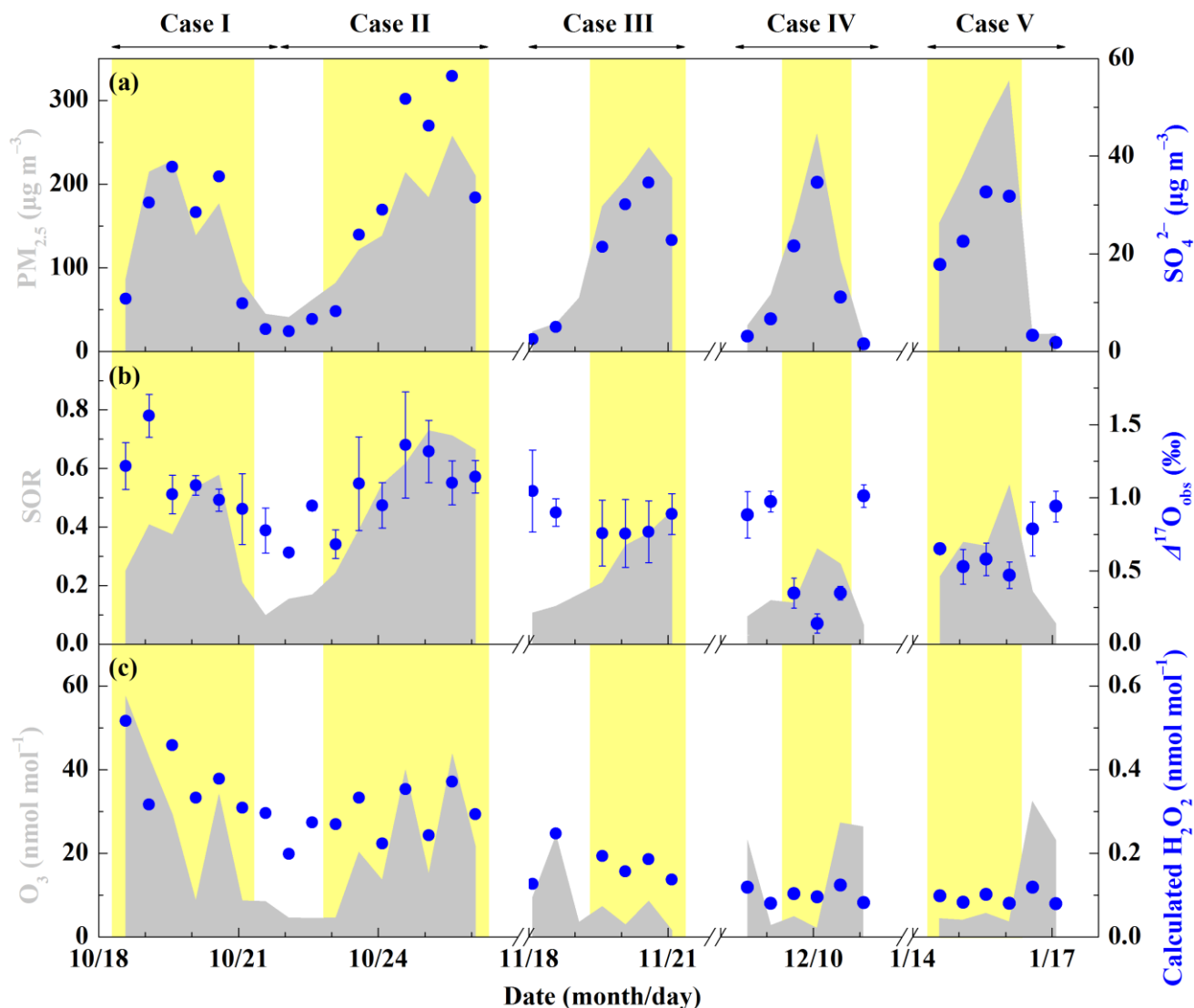
554 Wang, Y., Zhuang, G., Tang, A., Yuan, H., Sun, Y., Chen, S., and Zheng, A.: The ion chemistry and the source of PM_{2.5}
555 aerosol in Beijing, *Atmos. Environ.*, 39, 3771-3784, 2005.

556 Wang, Y., Zhang, Q., Jiang, J., Zhou, W., Wang, B., He, K., Duan, F., Zhang, Q., Philip, S., and Xie, Y.: Enhanced sulfate
557 formation during China's severe winter haze episode in January 2013 missing from current models, *J. Geophys. Res.*, 119,
558 10425-10440, 2014.

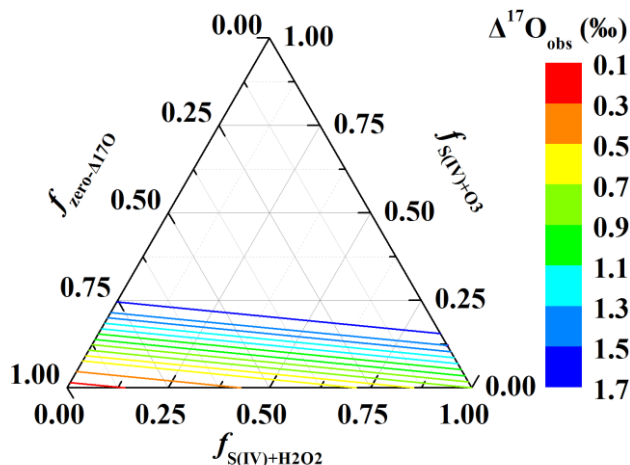
559 Ye, P., Xie, Z., Yu, J., and Kang, H.: Spatial distribution of methanesulphonic acid in the Arctic aerosol collected during the
560 Chinese Arctic Research Expedition, *Atmosphere*, 6, 699-712, 2015.

561 Zheng, B., Zhang, Q., Zhang, Y., He, K., Wang, K., Zheng, G., Duan, F., Ma, Y., and Kimoto, T.: Heterogeneous chemistry:
562 a mechanism missing in current models to explain secondary inorganic aerosol formation during the January 2013 haze
563 episode in North China, *Atmos. Chem. Phys.*, 15, 2031-2049, 2015a.

567 **Figures and Tables**

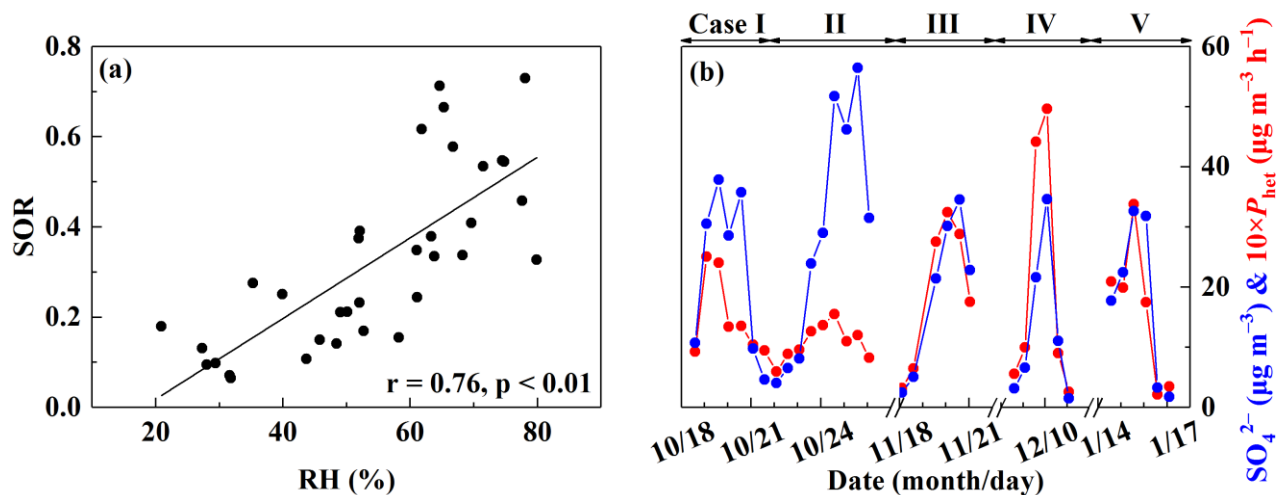


568
 569 **Figure 1.** Characteristics of haze events in Beijing (October 2014–January 2015). (a) Temporal evolution of $PM_{2.5}$ and SO_4^{2-}
 570 concentrations. (b) Temporal evolution of sulfur oxidation ratio (SOR, which equals to SO_4^{2-} molar concentration divided by
 571 the sum of SO_4^{2-} and SO_2 molar concentration) and observed $\Delta^{17}O(SO_4^{2-})$ ($\Delta^{17}O_{obs}$). (c) Temporal evolution of observed O_3
 572 and calculated H_2O_2 . The error bar of $\Delta^{17}O_{obs}$ in (b) is $\pm 1\sigma$ of replicate measurements ($n = 2-4$) of each sample. The light
 573 yellow shaded area indicates polluted days (PD, $PM_{2.5} \geq 75 \mu g m^{-3}$). Data used here are 12h-averaged values, corresponding
 574 with filter samples.



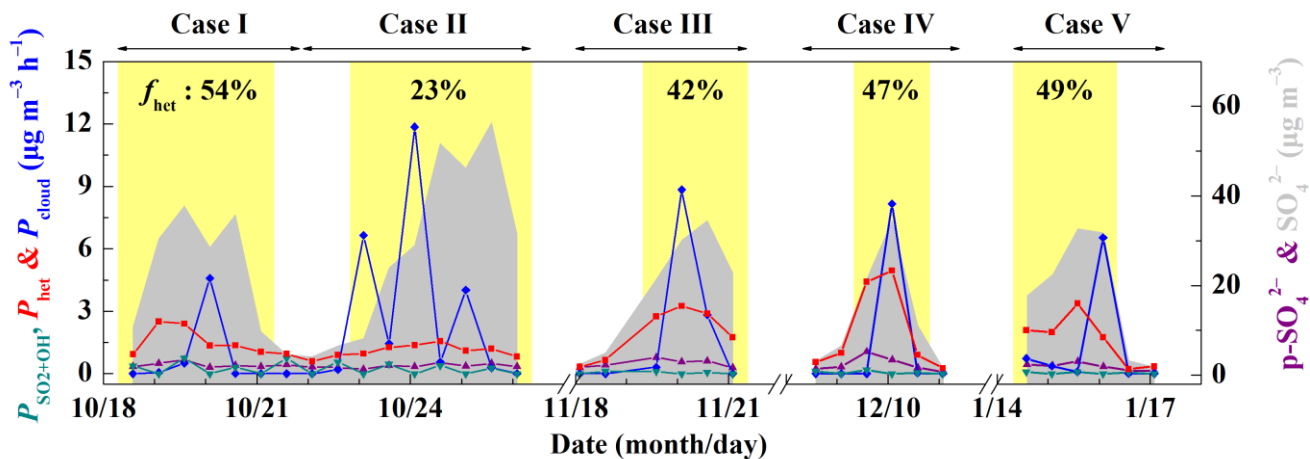
575

576 **Figure 2.** Ternary diagram of possible fractional contribution of different pathways to total sulfate production directly
 577 estimated from $\Delta^{17}\text{O}_{\text{obs}}$. The colored lines are contour lines of $\Delta^{17}\text{O}_{\text{obs}}$, representing possible fractional contribution of sulfate
 578 formation via O_3 ($f_{\text{S(IV)+O}_3}$) and H_2O_2 ($f_{\text{S(IV)+H}_2\text{O}_2}$) oxidation or zero- $\Delta^{17}\text{O}$ processes ($f_{\text{zero-}\Delta^{17}\text{O}}$) such as primary sulfate, secondary
 579 sulfate formed via OH oxidation, NO_2 oxidation and O_2 oxidation. $f_{\text{S(IV)+H}_2\text{O}_2}$ is in the range of 0 to $\min\{\Delta^{17}\text{O}_{\text{obs}}/0.7\text{‰}, (6.5\text{‰}-$
 580 $\Delta^{17}\text{O}_{\text{obs}})/5.8\text{‰}\}$, $f_{\text{S(IV)+O}_3} = (\Delta^{17}\text{O}_{\text{obs}} - 0.7\text{‰} \times f_{\text{S(IV)+H}_2\text{O}_2})/6.5\text{‰}$ and $f_{\text{zero-}\Delta^{17}\text{O}} = (6.5\text{‰} - \Delta^{17}\text{O}_{\text{obs}} - 5.8\text{‰} \times f_{\text{S(IV)+H}_2\text{O}_2})/6.5\text{‰}$. See
 581 equation 6 and its caption in Sect. 2.7 for details.



582

583 **Figure 3.** The relationship between relative humidity (RH) and SOR (a) and time series of overall heterogeneous sulfate
 584 production (P_{het}) along with SO_4^{2-} concentrations (b). The black line in (a) is linear least-squares fitting line.



585

586

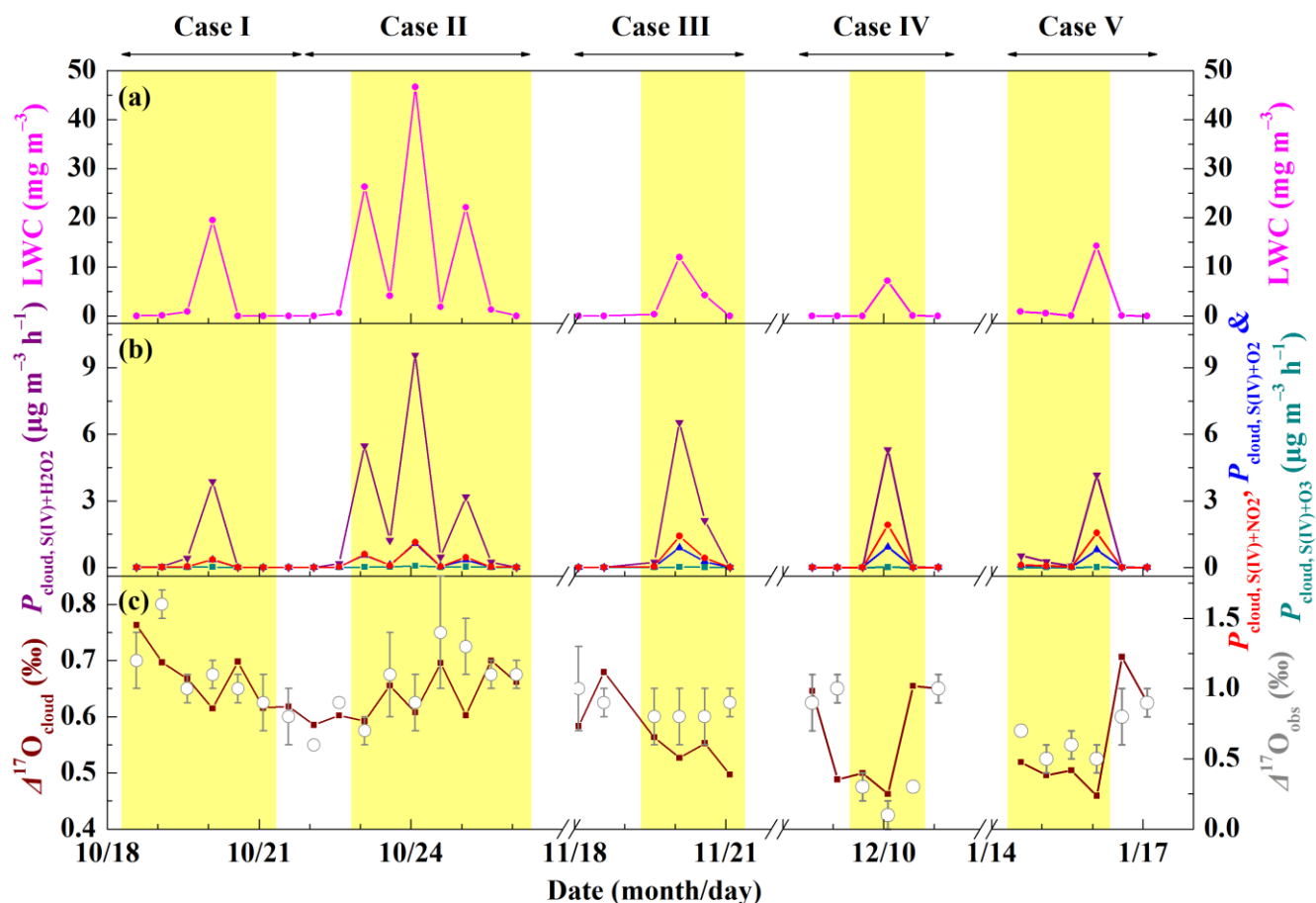
587

588

589

590

Figure 4. Estimate of different sulfate production pathways. Time series of estimated sulfate production rate via OH oxidation in the gas-phase (P_{SO_2+OH}), overall heterogeneous reactions on aerosols (P_{het}) and in-cloud reactions (P_{cloud}) and concentrations of primary sulfate ($p-SO_4^{2-}$) and observed sulfate. f_{het} represents the fraction of overall heterogeneous sulfate production to total sulfate production during PD of each Case. The light yellow shaded area indicates polluted days (PD, $PM_{2.5} \geq 75 \mu g m^{-3}$). Data used here are 12h-averaged values, corresponding with filter samples.



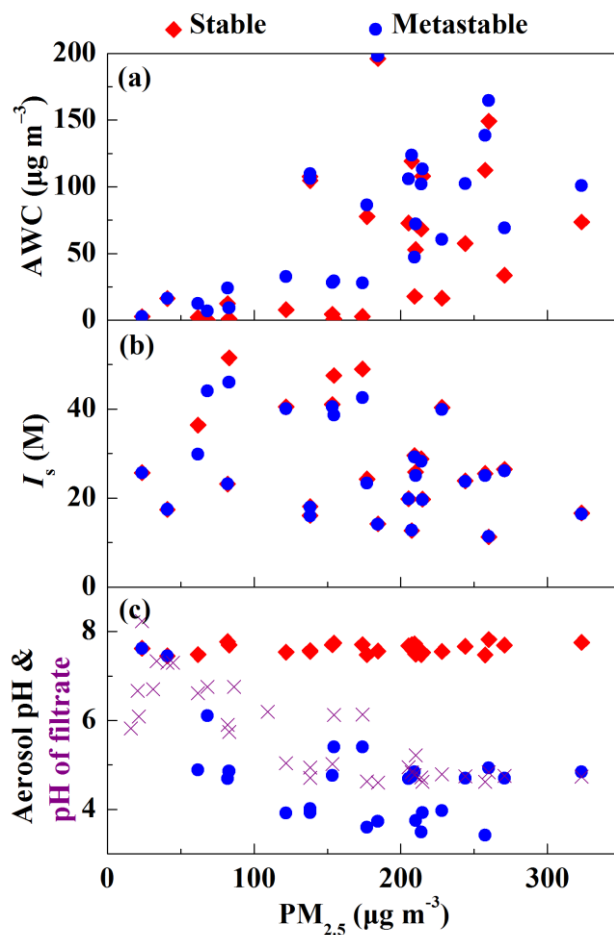
591

592

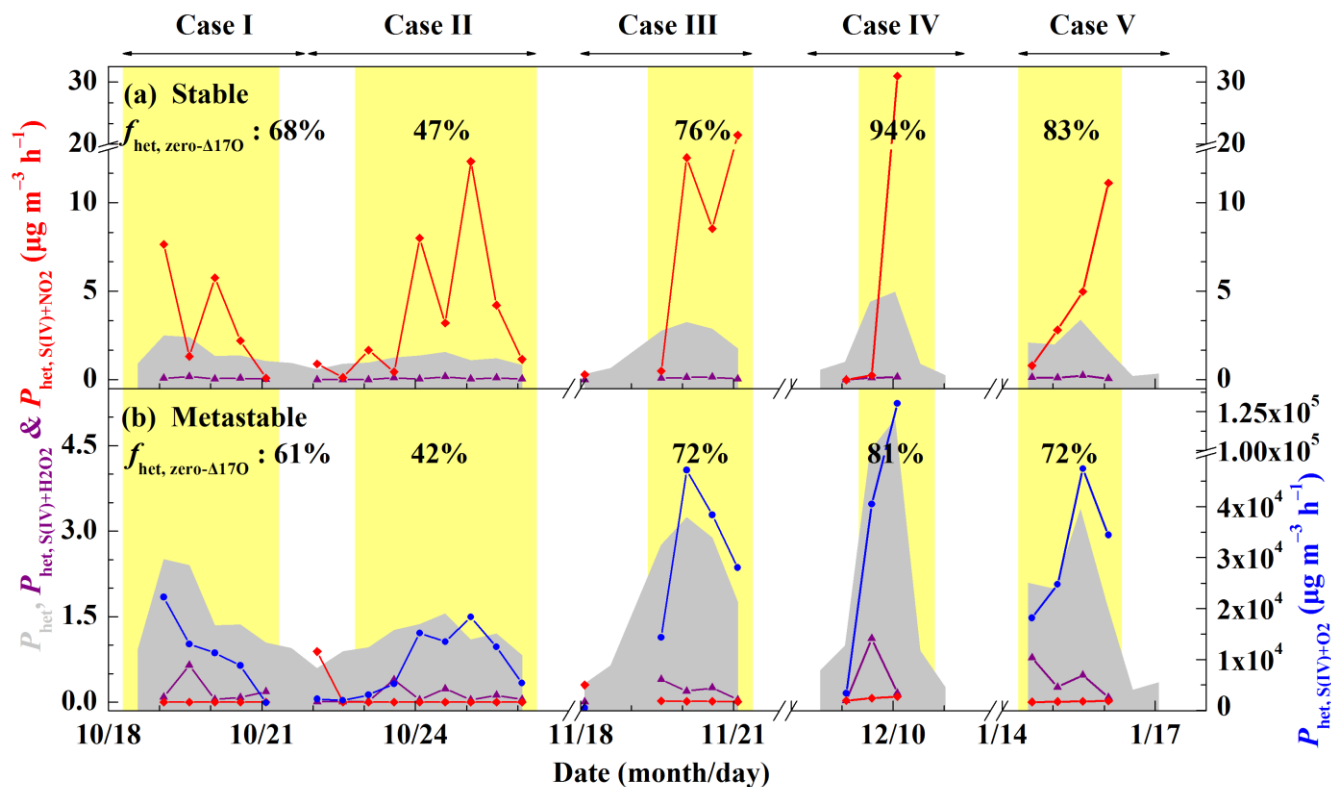
593

Figure 5. Temporal evolution of cloud liquid water content (LWC, a), in-cloud sulfate production rate via S(IV) oxidation by H_2O_2 , O_3 , NO_2 and O_2 initiated by TMIs (denoted as $P_{cloud, S(IV)+H_2O_2}$, $P_{cloud, S(IV)+O_3}$, $P_{cloud, S(IV)+NO_2}$ and $P_{cloud, S(IV)+O_2}$, respectively,

594 **b)** and estimated $\Delta^{17}\text{O}$ of sulfate produced in clouds ($\Delta^{17}\text{O}_{\text{cloud}}$, **c**). The light yellow shaded area indicates polluted days (PD,
595 $\text{PM}_{2.5} \geq 75 \mu\text{g m}^{-3}$). Data used here are 12h-averaged values, corresponding with filter samples.

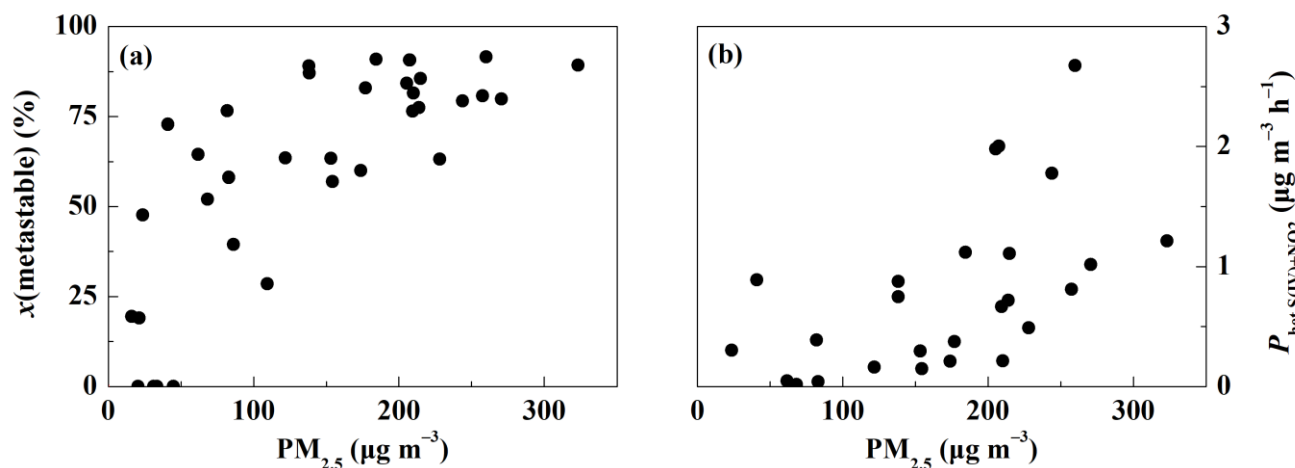


596
597 **Figure 6.** Aerosol parameters during Beijing haze. The aerosol liquid water content (AWC, **a**), ionic strength (I_s , **b**) and aerosol
598 pH (**c**) was predicted by ISORROPIA II assuming stable aerosol state and metastable aerosol state. The pH of filtrate was
599 measured by an ion activity meter.



600

601 **Figure 7.** Estimate of heterogeneous sulfate production pathways. Time series of overall heterogeneous sulfate production rate
 602 (P_{het}), heterogeneous sulfate production rate in aerosol water via H₂O₂ ($P_{het, S(IV)+H_2O_2}$) and NO₂ ($P_{het, S(IV)+NO_2}$) under stable (a)
 603 and metastable (b) aerosol assumption. $P_{het, S(IV)+O_2}$ in (b) represents heterogeneous sulfate production rate via SO₂ oxidation
 604 by O₂ via a radical chain mechanism on acidic microdroplets. $f_{het, zero-\Delta^{17}\text{O}}$ represents the fraction of heterogeneous reactions
 605 that result in sulfate with zero- $\Delta^{17}\text{O}$, such as S(IV) oxidation by NO₂ and O₂, to the overall heterogeneous sulfate production
 606 during PD of each case with the constraint of $\Delta^{17}\text{O}(\text{SO}_4^{2-})$ (see the main text for details). In calculating $P_{het, S(IV)+H_2O_2}$, the
 607 influence of I_s was considered. In calculating $P_{het, S(IV)+NO_2}$, and $P_{het, S(IV)+O_2}$ the influence of I_s was not considered due to the
 608 lack of experimental data about the influence of I_s . $P_{het, S(IV)+O_2}$ was calculated using the aqueous-phase rate constant for $\text{pH} \leq$
 609 3 due to the lack of rate constant information at $\text{pH} > 3$. The light yellow shaded area indicates polluted days (PD, $\text{PM}_{2.5} \geq 75$
 610 $\mu\text{g m}^{-3}$). Data used here are 12h-averaged values, corresponding with filter samples.



611

612 **Figure 8.** The estimated fraction of metastable aerosol to total aerosol ($x(\text{metastable})$, **a**) using Eq. (9) and heterogeneous
613 sulfate production rate from S(IV) oxidation by NO_2 assuming a combination of metastable and stable state ($P_{\text{het, S(IV)+NO}_2}$, **b**)
614 as $P_{\text{het, S(IV)+NO}_2} = x(\text{metastable}) \times P_{\text{het, S(IV)+NO}_2, \text{metastable}} + (100\% - x(\text{metastable})) \times P_{\text{het, S(IV)+NO}_2, \text{stable}}$.

615 **Table 1.** Sulfate isotope assumptions.

| Sulfate formation pathways | $\Delta^{17}\text{O}(\text{SO}_4^{2-})$ (‰) |
|---------------------------------------|---|
| $\text{SO}_2 + \text{OH}$ | 0 |
| $\text{S(IV)} + \text{H}_2\text{O}_2$ | 0.7 |
| $\text{S(IV)} + \text{O}_3$ | 6.5 |
| $\text{S(IV)} + \text{NO}_2$ | 0 |
| $\text{S(IV)} + \text{O}_2$ | 0 |
| Primary sulfate | 0 |

616 **Table 2.** Estimated fractional contribution of different sulfate production pathways during Beijing haze.

| PD of case | f_p (%) ^a | f_{het} (%) | f_{cloud} (%) | $f_{\text{SO}_2+\text{OH}}$ (%) |
|------------|------------------------|----------------------|------------------------|---------------------------------|
| I | 9 | 54 | 29 | 8 |
| II | 6 | 23 | 68 | 3 |
| III | 11 | 41 | 47 | 1 |
| IV | 15 | 47 | 37 | 1 |
| V | 9 | 49 | 41 | 1 |

617 ^a f_p , f_{het} , f_{cloud} , and $f_{\text{SO}_2+\text{OH}}$ respectively represents fractional contribution from primary sulfate, heterogeneous reactions, in-
618 cloud reactions and gas-phase pathway.